

# MicroBooNE Proposal Addendum

March 3, 2008

H. Chen, G. de Geronimo, J. Farrell, A. Kandasamy, F. Lanni, D. Lissauer, D.

Makowiecki, J. Mead, V. Radeka, S. Rescia, J. Sondericker, B. Yu

*Brookhaven National Laboratory, Upton, NY*

L. Bugel, J. M. Conrad, Z. Djurcic, V. Nguyen, M. Shaevitz, W. Willis<sup>†</sup>

*Columbia University, New York, NY*

C. James, S. Pordes, G. Rameika

*Fermi National Accelerator Laboratory, Batavia, IL*

C. Bromberg, D. Edmunds

*Michigan State University, Lansing, MI*

P. Nienaber

*St. Mary's University of Minnesota, Winona, MN*

S. Kopp, K. Lang

*University of Texas at Austin, Austin, TX*

C. Anderson, B. T. Fleming<sup>†</sup>, S. Linden, M. Soderberg, J. Spitz

*Yale University, New Haven, CT*

<sup>†</sup>= Spokesperson, <sup>‡</sup>= Deputy Spokesperson

# Contents

<b>1</b>	<b>Introduction</b>	<b>1</b>
<b>2</b>	<b>Expanding on the Physics Motivation of MicroBooNE</b>	<b>5</b>
2.1	Update on the MiniBooNE low energy excess . . . . .	5
2.1.1	Brief Overview of MiniBooNE . . . . .	6
2.1.2	BNB Beam Results . . . . .	8
2.1.3	NOA Beam Results . . . . .	17
2.1.4	Summary of the Status of the Low Energy Excess . . . . .	18
2.1.5	Impact of Low Energy Excess on Broader Program . . . . .	20
2.1.6	Addressing the Low Energy Excess at MicroBooNE . . . . .	22
2.2	Update on Low Energy Neutrino Cross Sections . . . . .	22
2.3	New: Measurements Relevant to an LAr Proton Decay Detector . . . . .	22
<b>3</b>	<b>Liquid Argon TPC Research and Development Towards Massive Detectors</b>	<b>25</b>
3.1	Detector R&D . . . . .	27
3.1.1	Purification . . . . .	28
3.1.2	Readout Electronics . . . . .	30
3.2	Physics R&D . . . . .	32

3.2.1	Physics Development . . . . .	33
3.2.2	Analysis Tools . . . . .	33
<b>4</b>	<b>Baseline Design Update</b>	<b>34</b>
4.1	Cryostat and Cryogenics . . . . .	35
4.1.1	Cryostat . . . . .	36
4.1.2	Feedthroughs . . . . .	37
4.2	TPC Detectors: Wires, HV, and Drifting Field . . . . .	38
4.2.1	High Voltage and Drifting Field . . . . .	38
4.2.2	Wire Termination . . . . .	38
4.2.3	Wire Mechanical Properties Comparison . . . . .	39
4.3	Readout Electronics and DAQ . . . . .	40
4.4	Summary . . . . .	43
<b>5</b>	<b>Overview of MicroBooNE Cost, Schedule, and Siting</b>	<b>46</b>
<b>6</b>	<b>Conclusions</b>	<b>51</b>
	<b>Bibliography</b>	<b>52</b>

# Chapter 1

## Introduction

The MicroBooNE collaboration presented a proposal for the MicroBooNE experiment to the Fermilab Physics Advisory Committee in Fall, 2007 [1]. The experiment has since evolved, guided by the recommendations of the committee and the Fermilab directorate and by advancement of our own studies. Presented here is an addendum to the MicroBooNE proposal describing the present status and trajectory of the experiment.

The recommendations from the committee were as follows:

“The MicroBooNE proposal involves the construction and operation of a new liquid argon TPC on the Booster Neutrino Beamline. The physics goals are to investigate the low-energy excess observed by MiniBooNE and to study low-energy neutrino cross-sections relevant to interpretation of future neutrino oscillation data. In addition, the construction and operation of the TPC are envisioned as steps in the development of future large (100 kTon) scale liquid argon TPC’s for long-baseline neutrino studies and proton decay searches.

The proposed plan for implementation of this detector as a physics experiment was not adequate for Stage 1 approval at this time. The construction schedule and project plan were judged to be unrealistic. In addition, the question of how the project would address the physics goals, given a realistic beam delivery schedule,

was not fully developed. Additional information from MiniBooNE regarding the significance of the low-energy excess should be helpful in further developing the physics case.

The Committee considers R&D towards large scale liquid argon TPC's to be a very important activity. However, the committee was not convinced that constructing the MicroBooNE detector was the optimal approach for R&D towards much larger devices. For example, individual issues such as contamination of the liquid argon by electronics components could be studied with smaller test setups.”

The MicroBooNE physics case has been strengthened by the growing interest in the MiniBooNE low energy excess, demonstrated by new phenomenology papers appearing on the archive and by dedicated sessions at conferences such as Moriond. After continuing study of the low energy excess within MiniBooNE and the community, the background predictions have been verified, with only small modifications. Results from the NuMI-line neutrino interactions in the MiniBooNE detector have been recently made public, presented at Fermilab in December, 2007.

With the rising prospect of using LArTPCs for next generation long baseline oscillation experiments, there is growing interest in measuring neutrino cross sections on argon. These measurements are important for neutrino oscillation measurements, and will also be useful for constraining particle identification kinematics for proton decay searches. The beams available – the Booster Neutrino Beam, and the NuMI off-axis beam (LE or ME) — are appropriate for measuring low energy neutrino cross sections.

Lastly, we introduce a new topic: measurements of value to a future LAr-based proton decay detector searching for  $p \rightarrow \nu k$ . Such a detector is likely to be part of the DUSEL program [2]. MicroBooNE provides a preliminary sample of  $\sim 480$  kaons from the BNB for study in preparation for proposing such a detector.

In Chapter 2, we present an expanded discussion of the physics motivation for MicroBooNE. As per the request of the PAC, we review the status of the MiniBooNE low energy excess, assembling the available published and public-but-preliminary information. We touch on the

physics of neutrino scattering from argon. Finally, we introduce measurements important to a future LAr proton decay experiment.

The collaboration has been deeply involved with the development of designs for multi-kiloton detectors. As we refine the design for MicroBooNE, we have addressed how natural extensions of this design can lead to optimum designs for larger detectors. Because of this and in response to the PAC's concerns regarding MicroBooNE's R&D goals and the broader liquid argon detector program, the MicroBooNE collaboration has significantly expanded the experiment's R&D goals.

The MicroBooNE R&D program will proceed in two, overlapping phases. The initial R&D phase already underway addresses design questions specific to the MicroBooNE detector. A second R&D phase will address longer term R&D questions relevant for the next stage of LArTPC detectors, the multi-kiloton scale. There is substantial overlap between these two phases in terms of the issues they address although the timing of each are different. The key issues to be addressed in MicroBooNE's second R&D phase are:

- Achieving purity using an un-evacuated cryostat
- Developing cold electronics for next generation LArTPCs
- Implementing general detector design appropriate for the next phase in the LArTPC program

The staging of the MicroBooNE experiment with two R&D phases allows for the successful combination of R&D and physics goals within the experiment.

Concurrent with the broadening in scope of the MicroBooNE R&D program over the last six months, there has been substantial progress in the planning for the US long baseline neutrino oscillation physics program. A series of workshops devoted to Project X physics [3] has explored and evaluated long baseline physics including the liquid argon detector program's role in this program. The evolution of the US Liquid argon TPC program in light of this longer term future has come into focus. MicroBooNE is a key component in this program providing the R&D necessary to ready the technology for the long baseline program. This is described in the

“Golden Book” writeup of the workshop series and supporting documents [4]. This program has been presented by the Project X conveners and the laboratory to the community and the DOE/NSF P5 committee [5]. A detailed description of the evolution of the LArTPC program in the US and MicroBooNE’s role in this program is given in Chapter 3.

Advances in design work as a result of value engineering and MicroBooNE’s R&D program have led to changes to the MicroBooNE detector design. An update of the baseline design of the detector is described in Chapter 4.

In response to the PAC’s concerns regarding MicroBooNE’s implementation plan, the collaboration has further developed the construction schedule and project plan. These are briefly described in Chapter 5; a detailed breakdown of each can be found on the MicroBooNE website [6].

## Chapter 2

# Expanding on the Physics

## Motivation of MicroBooNE

MicroBooNE employs a  $\sim 70$  ton fiducial volume Liquid Argon Time Projection Chamber (LArTPC), which offers excellent discrimination between photons and electrons and good particle identification in general. The high spatial resolution and energy measurement down to the MeV scale provides information for low and high energy particles that has not been available using high intensity beams. MicroBooNE is therefore extremely well suited to addressing the low energy excess observed by the MiniBooNE experiment and measuring low energy neutrino cross sections on argon. This section describes the physics motivation for MicroBooNE, focusing on aspects developed and clarified since submission of the original proposal.

### 2.1 Update on the MiniBooNE low energy excess

The MiniBooNE Collaboration has reported a  $3.7\sigma$  excess of events which were characterized as “electron-like” in the neutrino data sample from the Booster Neutrino Beam (BNB) [7]. This excess is not consistent with two neutrino  $\nu_\mu \rightarrow \nu_e$  oscillations. Using the same cuts, an excess of events is also reported in the sample from the NuMI off-axis (NOA) beam [8], although at lower significance ( $1.4\sigma$ ).

This section reports experimental aspects of the two measurements of an excess of events at low energy. It is shown that the excess is not due to  $\pi^0$  interactions or other presently identified backgrounds. Information on energy and angular distributions is provided.

The organization of this section is as follows:

1. The aspects of the MiniBooNE design which are relevant to the discussion are reviewed.
2. The public information on the MiniBooNE low energy excess observed in the BNB line is reported.
3. The public information on the excess observed in the NuMI line, as drawn from the Joint Theoretical-Experimental Seminar (“Wine and Cheese”) presented on Dec. 11, 2007, is discussed. It should be noted that these results, while public, are preliminary and not published.

### 2.1.1 Brief Overview of MiniBooNE

The BNB and NOA beams have been described in Chapter 3 of the MicroBooNE proposal [1]. For this discussion it is useful to re-iterate two features of the NOA beam: it is 110 mrad off-axis and, given the energy cuts applied in the analysis, the neutrinos originate from the NuMI target region and thus have a well defined origin. In both analyses, the  $z$ -axis is defined as along the beam direction. Thus, the  $z$ -axis for the NOA beam is rotated with respect to the BNB beam. The  $y$ -axis is always defined as upward with respect to the  $z$ -axis. The  $x$ -axis completes a right-handed coordinate system.

The timing of the BNB and NOA beams are designed so that the spills will not overlap. In both cases, the MiniBooNE trigger is a 19.6  $\mu\text{s}$  window which surrounds the 1.6  $\mu\text{s}$  BNB beam spill and the 10  $\mu\text{s}$  NuMI spill.

The events in the MiniBooNE detector are simulated using the v3 NUANCE Monte Carlo Event Generator[9]. For comparisons below, “cocktail Monte Carlo,” which has the correct mix of event-type versus energy for the MiniBooNE flux, is shown. Some parameters of this Monte Carlo were tuned to reproduce the observed kinematics of charged current quasi-elastic

(CCQE) events from the BNB in the MiniBooNE detector [10]. These were also used in the NOA beam analysis. The subsequent simulation of the events in the detector uses GEANT3 [11] with thresholds set to 10 keV, thus allowing subsequent electromagnetic radiation as charged particles propagate. GICALOR [12] is used to model hadronic interactions. The simulation of light production and propagation in mineral oil has been tuned using external measurements [13], muon decay electrons (also used to calibrate the energy scale), and recoil nucleons from neutrino neutral current (NC) elastic scattering events. Data taken during the beam-off gate are overlaid on simulated events to account for cosmic rays and natural radioactivity in the tank.

“Precuts” are applied to remove cosmic ray and other non-beam-related backgrounds. The initial neutrino interaction is required to occur within the beam window, to have fewer than 6 veto hits, and more than 200 phototube hits out of 1282. After precuts, the BNB and NOA beam event samples are similar. The  $\nu_\mu$  CCQE content for BNB (NOA) is 39% (48%), charged current single  $\pi^+$  is 26% (31%) and neutral current single  $\pi^0$  is 9% (8%).

The analysis searches for events which are consistent with  $\nu_e$  CCQE interactions. These have a single electron track and, in some cases, scintillation light from the hadronic vertex. There is no muon in the event, hence no decay Michel electron from the muon. Thus, activity only at the initial neutrino interaction (the “first subevent”) is required.

For the NuMI analysis, the “track-based” reconstruction for the MiniBooNE oscillation result [7, 14], was used. This reconstruction assumes that light is produced by an extended source. For each event, a vertex position, angle, energy and time of the event are reconstructed assuming a single track. In order to assure that the event is in kinematic and spatial regions where events are well-simulated, two further cuts, using reconstructed information, are then applied. The visible energy in the tank is required to be  $E_{vis} > 140$  MeV. The vertex is required to be within 500 cm of the center of the tank.

A likelihood-based analysis [14] is employed to distinguish events which have a high probability of being a single electron track. The likelihoods are constructed based on phototube charge and time PDFs. The event is first reconstructed under a single-track hypothesis and then tested for the likelihood that it is electron-like ( $L_e$ ) and muon-like ( $L_\mu$ ). The event is then

$E_\nu^{QE}$ [MeV]	200-300	300-475	475-1250
total background	284±25	274±21	358±35
$\nu_e$ intrinsic	26	67	229
$\nu_\mu$ induced (“Mis-ID”)	258	207	129
NC $\pi^0$	115	76	62
NC $\Delta$ rad	20	51	20
Dirt	99	50	17
other	24	30	30
Data	375±19	369±19	380±19
Data-background	91±31	95±28	22±40

Table 2.1: Information on the excess observed in the BNB line as a function of three energy bins. Row two shows the total background. Rows three and four divide the backgrounds between intrinsic  $\nu_e$  and mis-identified (“Mis-ID”) events. Rows 5 through 8 break out the Mis-ID contributions. Row 9 gives the measurement. Row 10 presents the excess.

reconstructed under a two track hypothesis, where the invariant mass of the two tracks is forced to be 135 MeV. This permits a neutral pion likelihood ( $L_\pi$ ) to be formed. Lastly, the event is reconstructed finding the best two track fit with no invariant mass requirement. This yields a best-fit mass ( $M$ ). Three visible-energy dependent cuts on  $\log(L_e/L_\mu)$ ,  $\log(L_e/L_\pi)$  and  $M$ , are then employed, as shown in ref. [14].

## 2.1.2 BNB Beam Results

### Signature of the Excess

Given single-track, electron-like events, MiniBooNE can reconstruct the neutrino energy assuming the event is  $\nu_e$  CCQE:

$$E_\nu^{QE} = \frac{2(M_n - E_B)E_e - (E_B^2 - 2M_n E_B + m_e^2 + \Delta M^2)}{2[(M_n - E_B) - E_e + p_e \cos \theta_e]}. \quad (2.1)$$

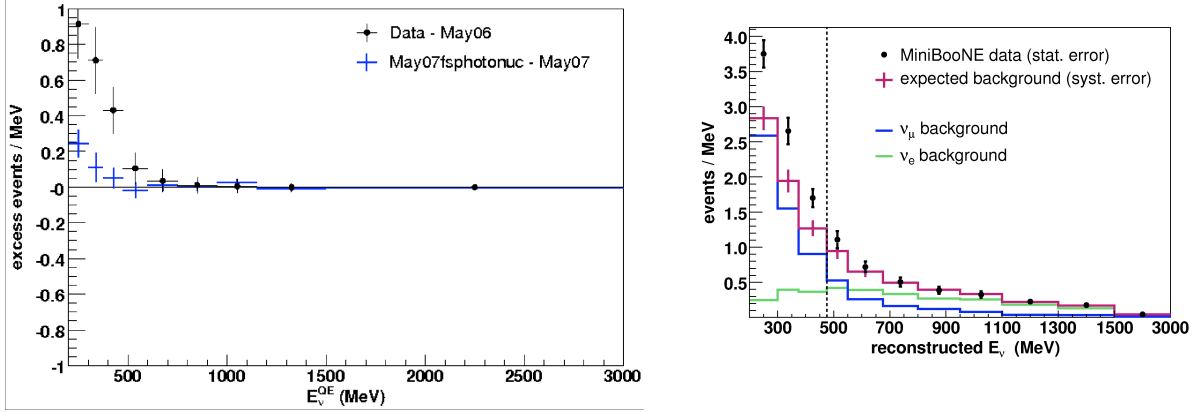


Figure 2.1: Left — Black: Excess (Data-MC) events reported by MiniBooNE in the first analysis [7]. Blue: Conservative **preliminary** estimate of contribution from photo-nuclear interactions, not included in the first analysis MC (see text). If the preliminary estimate of this new background stands, the remaining excess will be black minus blue. Right – Data distribution compared to absolutely normalized Monte Carlo. **Premininary** additional bin from 200-300 is shown. Red: total predicted background from first analysis Monte Carlo. Blue:  $\nu_{\mu}$  Mis-ID background. Green:  $\nu_e$  intrinsic background.

In this equation,  $m_e$  is the electron mass,  $E_e(p_e)$  is the electron reconstructed energy (momentum),  $\theta_e$  is the reconstructed scattering angle,  $E_B = 34$  MeV [10], and  $\Delta M^2 = M_n^2 - M_p^2$ . A small correction is applied to  $E_\nu$  to account for the biasing effects of Fermi-smearing.

Figure 2.1 (top), shows the excess (Data–MC) e-like events as a function of  $E_{QE}^\nu$  presented in the MiniBooNE published oscillation analysis [7], indicated by the black crosses (the blue crosses are explained in later text). Figure 2.1 (bottom) directly compares data to absolutely normalized Monte Carlo. In Figure 2.1 (bottom) one additional preliminary bin beyond the published result, from 200 to 300 MeV, is presented [15]. A clear excess of events above expectation is observed. The change in the excess from the 200 to 300 MeV bin to the next bin is consistent, within errors, with the change in the neutrino flux.

Studies of various low-level-detector and physics distributions have produced no clear clues on the source of the excess [16]. There is no evidence of this excess in the beam-off data.

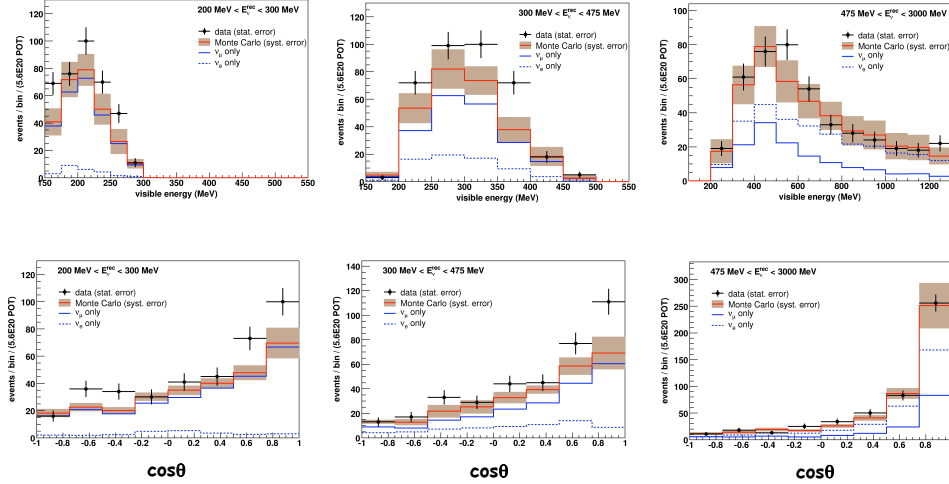


Figure 2.2: **Preliminary:** Top Row – visible energy distribution of electron-like events in the tank for three  $E_{\nu}^{QE}$  ranges. Bottom Row – angular distributions for the same ranges.

There was a study of low-level hit information to assure that this is not a detector effect. The distribution of visible energy in the tank for the event sample is shown in Figure 2.2 (top row) for three  $E_{\nu}^{QE}$  bins, while the  $\cos\theta$  angular distribution is shown in Figure 2.2 (bottom row) [15]. Conclusions on these distributions are limited by statistics, but there are no obvious non-electron-like trends in the excess. The event displays for electron-like events with  $E_{\nu}^{QE} < 500$  MeV were hand-scanned. It was found that 92% of the events were consistent with the expectation of single-ring electromagnetic showers. An event display is shown in Figure 2.4.

## Backgrounds

Table 2.1 breaks down the sources of backgrounds in the BNB analysis as a function of energy. This table was presented to the PAC in autumn, 2007, in the MiniBooNE “Request for Further Anti-Neutrino Running” [17]. The largest backgrounds are from intrinsic  $\nu_e$ ’s from the beam and mis-identification of  $\nu_{\mu}$  events in the detector. The mis-identified  $\nu_{\mu}$  events come largely from three sources:  $\pi^0$  decay where one photon is not reconstructed, radiative decay of the  $\Delta$  and events in the surround material (“dirt”) which produce a single photon entering the detector.

Comparing the shape of the excess as a function of energy to each of these backgrounds, one can see that these backgrounds do not have the appropriate energy dependences to match the energy dependence of the excess. However, it is worthwhile to consider each of these sources in detail.

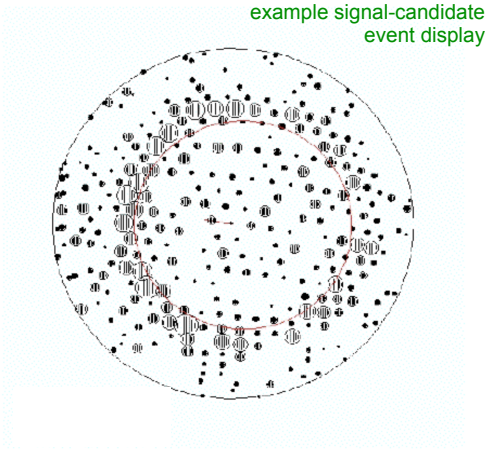


Figure 2.3: Event display of a data event in the low energy excess region.

The other major source is the case where a photon exits the tank. This is straightforward to model given an accurate measurement of the conversion length and the interaction vertex distribution.

A crucial technique for the MiniBooNE oscillation result constrains the background from  $\pi^0$  decays using the reconstructed  $\pi^0$  events observed in the detector. This is described in a paper which is soon to be published by the MiniBooNE Collaboration [18]. Because MiniBooNE reconstructs 99% of the  $\pi^0$ 's, which can be binned as a function of the  $\pi^0$  momentum, MiniBooNE can very accurately determine this Mis-ID rate. The Mis-ID'd events are at the 1% level and the error on the knowledge of this 1% is less than 10%. Note that this method, which uses the *rate* of  $\pi^0$  events observed in the detector, does not suffer from systematics due to predicting the flux or cross section. It only suffers from errors due to measuring the absolute rate of events. This is a very robust method.

One aspect of  $\pi^0$  mis-identification that was not included in the MiniBooNE Monte Carlo

From this table, one can see that a significant source of background to the MiniBooNE BNB analysis is from  $\pi^0$  Mis-IDs. These come mainly from back-to-back  $\pi^0$  decays which produce one high energy electromagnetic ring in the detector and one low energy (or “weak”) ring. If the weak ring is not reconstructed, then the event will be identified as an electromagnetic shower. This Mis-ID rate is, therefore, driven by the kinematics of the  $\pi^0$  decay, which are straightforward to model if one knows the momentum distribution of the  $\pi^0$ 's which are

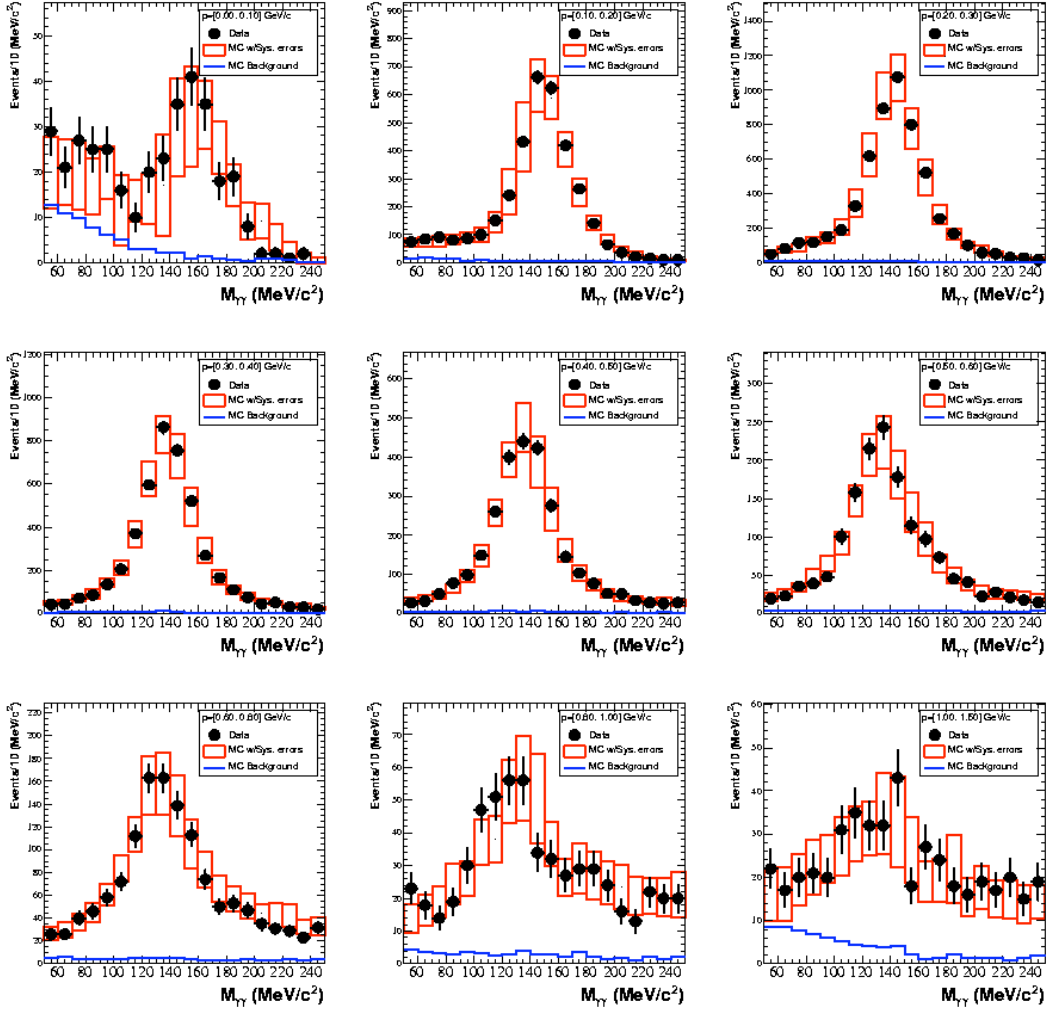


Figure 2.4: Invariant mass peaks of the identified  $\pi^0$  distributions as a function of  $\pi^0$  momentum. Monte Carlo was adjusted such that  $\text{flux} \times \text{cross section}$  matched the data distribution. For details see ref. [7].

for the published analysis is due to photo-nuclear interactions of the daughter photons. In these interactions, one photon from the  $\pi^0$  is lost because it interacts with nuclei in the tank. In these interactions, the photon can be absorbed by the nucleus and, thus, change a two photon event into a single photon event. In the absorption process the nucleus can emit secondary pions or gammas. These secondary particles can emit light in the detector that causes many of these events to be rejected as electron-like candidates, but a small number can pass the electromagnetic shower classification by the likelihood cuts. The cross section is relatively small, with two peaks: one at 23 MeV which is 20 mb (called the “Giant Dipole Resonance”) and the other at about 300 MeV which is 5 mb (the  $\Delta$  resonance). Even though these interaction rates are small, recent studies have shown that they can produce mis-identified events at low visible energies. Great effort has gone in to MiniBooNE’s recent work to model this effect, which is not in GEANT3. It is difficult to isolate a sample of test events on which to test the model, and so MiniBooNE has been generous in its estimates of rates and conservative in its assignment of error. The blue data points on Figure 2.1(top) show the contribution from this source. This estimate accounts for 13% of the excess above 300 MeV and 27% of the excess from 200-300 MeV. If this analysis continues to bear out, then the MiniBooNE excess would be the difference between the published excess (black) and the additional background estimate (blue).

The radiative delta decay is a small contribution to the total error. However, once the  $\pi^0$  rate is constrained by the data, the rate of radiative decay events is also constrained.

Another important background to the analysis is from the neutrino interactions in the material surrounding the MiniBooNE detector; this background is referred to as the “dirt.” background. The primary source of background for the appearance search are photons which enter the tank from neutrino interactions outside the tank. These events can be well-constrained because they appear predominantly near the wall of the tank and thus isolated and studied. Before the MiniBooNE “box” was opened, a sample of dirt events was isolated, to allow confirmation of the Monte Carlo [7]. Examples of plots which were used to cross-check the dirt Monte Carlo are shown in Fig 2.5, along with a pie chart indicating the sources of dirt photons.

At low energies the primary contribution to the intrinsic  $\nu_e$  background is from muon decay.

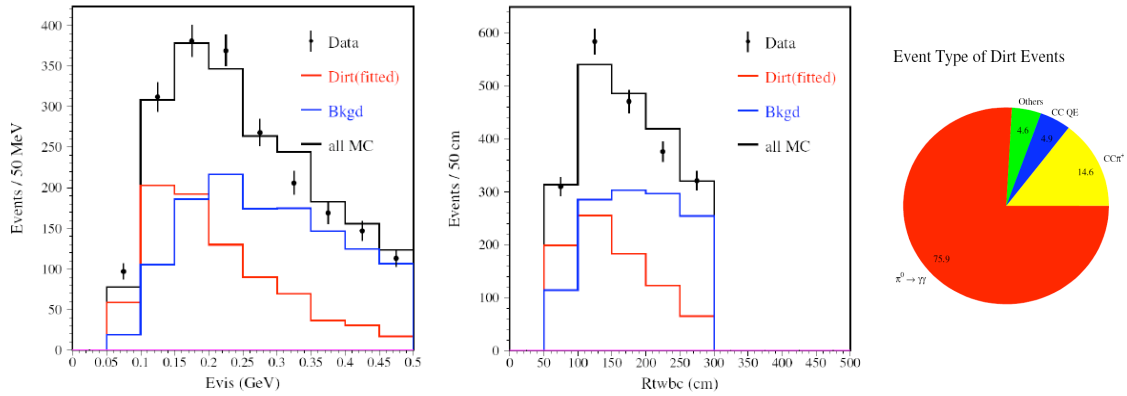


Figure 2.5: Two histograms used to check the “dirt” Monte Carlo prediction. The Monte Carlo is absolutely normalized. The actual dirt contribution is shown in red. The distributions used as cross checks were chosen for the difference in the shape of the dirt distribution compared to in-tank events (blue). The pie chart indicates the relative sources of dirt events. For further discussion see ref. [7]

MiniBooNE constrains the  $\nu_e$  from muon decay in the beam using the observed  $\nu_\mu$  events. This method works because the MiniBooNE detector subtends a small solid angle aligned along the beam direction. As a result, the geometry picks out forward decays in the COM system where the neutrino goes along the pion direction. This leads to a strong correlation between the  $\nu_\mu$  energy and the  $\pi^+$  energy. Once one has properly modeled the  $\pi^+$  energy distribution, modeling the muon produced in the decay and the subsequent electron neutrino rate from this decay is straightforward [19]. The predicted  $\nu_e$  from kaon decay comes from fits to secondary meson production. This was cross checked by comparing the observed versus predicted rate of high energy  $\nu_\mu$  events, which come predominately from kaon decays [7].

In summary, after eight months of study following the “box-opening”, MiniBooNE has not identified a Standard Model source or background that explains the MiniBooNE observed excess in the BNB beam.

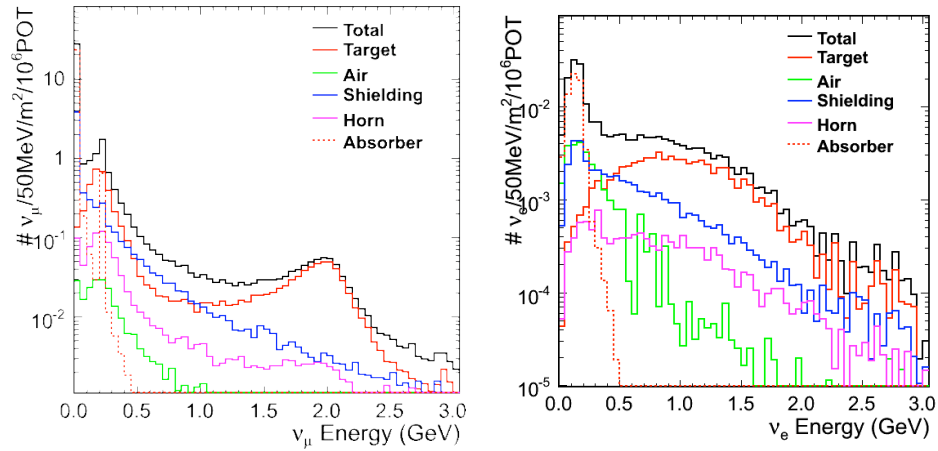


Figure 2.6: Sources of neutrinos seen in the MiniBooNE detector produced in the NuMI line.

Left –  $\nu_\mu$ ; Right –  $\nu_e$ .

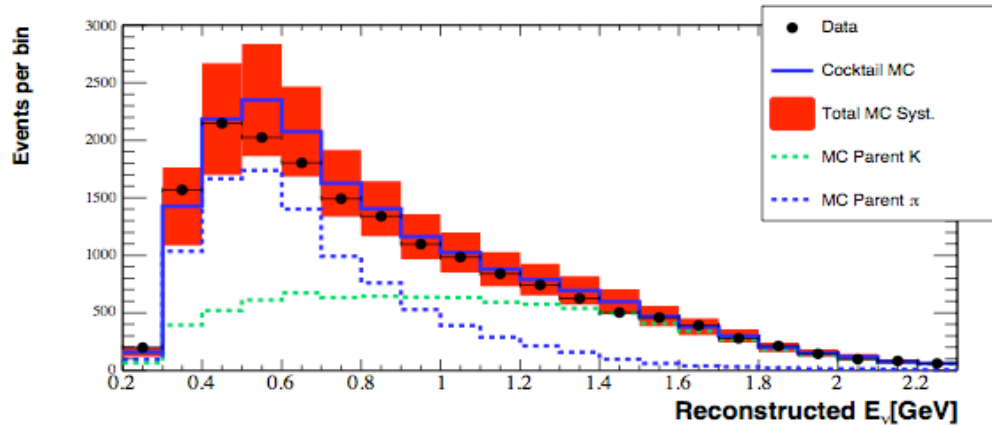


Figure 2.7: **Preliminary:** NOA  $\nu_\mu$  CCQE interactions compared to absolutely normalized “Cocktail MC,” which refers to Monte Carlo with all event sources. Systematic errors are indicated by the red band. Contribution from pion decay is indicated in blue; kaon decay is indicated in green.

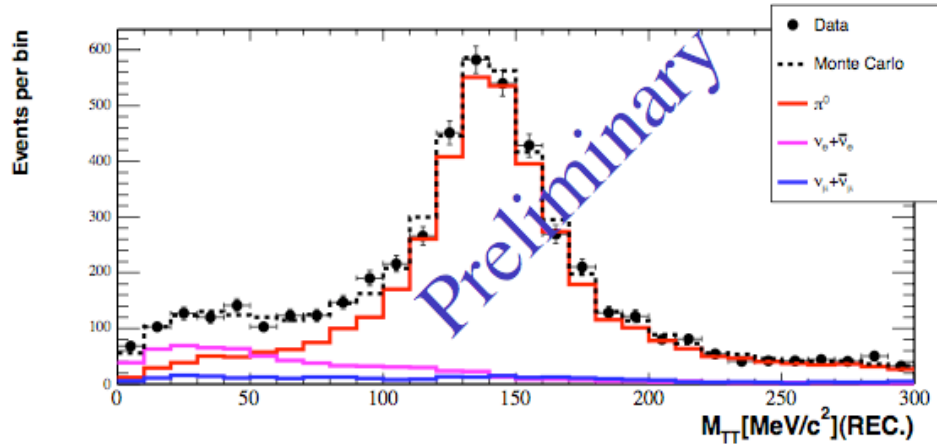


Figure 2.8: **Preliminary:** NOA  $\pi^0$  invariant mass peak compared to absolutely normalized “Cocktail” Monte Carlo. The contribution from true  $\pi^0$  events is indicated in red. The contribution from  $\nu_e$  and  $\bar{\nu}_e$ , which tend to reconstruct at low invariant mass is indicated in magenta. Other backgrounds are indicated in blue.

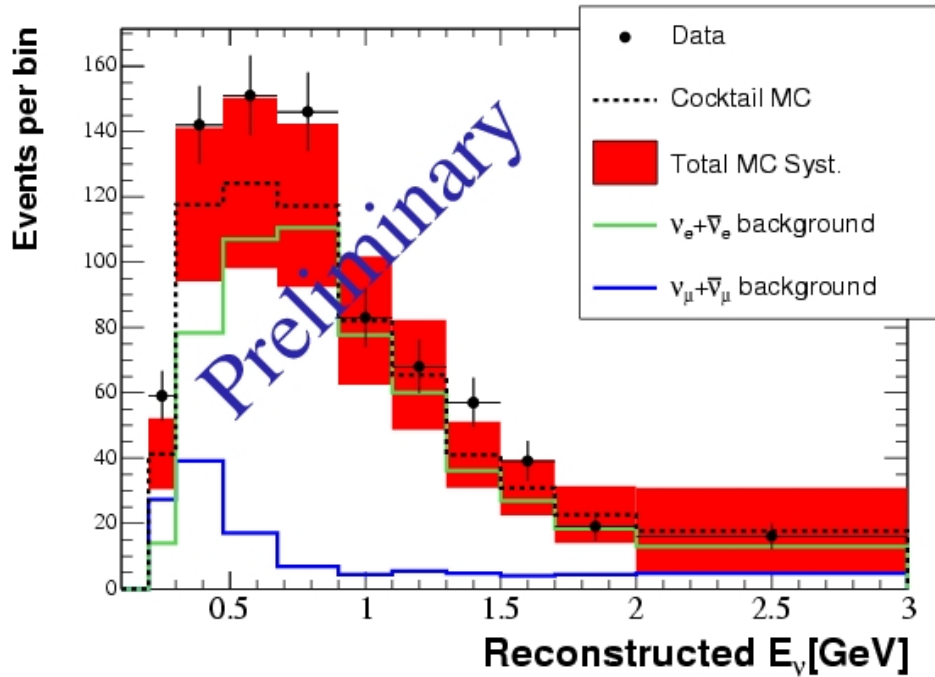


Figure 2.9: **Preliminary:** NOA  $\nu_e$  interactions compared to absolutely normalized “Cocktail” Monte Carlo. Systematic errors are indicated by the red band. Contribution from true  $\nu_e$  and  $\bar{\nu}_e$  events is shown in green. Contribution from  $\nu_\mu$  and  $\bar{\nu}_\mu$  Mis-ID is shown in blue.

### 2.1.3 NOA Beam Results

As stated above, MiniBooNE has also made measurements using off-axis neutrinos from the NuMI beam. Figure 2.6 shows the predicted sources of NuMI neutrinos observed in the MiniBooNE detector. Because of the layout of the NuMI beam relative to the MiniBooNE detector and the short decay length of kaons, the  $\nu_\mu$  flux comes almost entirely from the target and shielding region. Thus these neutrinos are emitted along a well defined angle and with a well defined length,  $L$ . The  $\nu_e$  flux has two important sources. First, below  $\sim 200$  MeV, there is a peak of  $\nu_e$  emitted by stopped kaons in the NuMI-line beam dump which is immediately below the MiniBooNE detector. In the analysis, these events are eliminated by increasing the visible energy cut to  $E_{vis} > 200$  MeV. This leaves  $\nu_e$  events which are produced by  $k$  decays in the target and shielding region of the NuMI beamline. Thus the  $\nu_e$ , like the  $\nu_\mu$ , comes from a well-defined source.

The analysis proceeded as with the BNB analysis:

- $\nu_\mu$  CCQE events were isolated and compared to the Monte Carlo prediction.
- The systematics were assigned. In particular, this required a  $\pi^0$  cross check described below.
- The  $\nu_e$  CCQE analysis then follows.

The same reconstruction and cuts, except for the higher  $E_{vis}$  cut explained above, are used for the NOA and BNB analyses. A difference between the BNB and NOA analyses was that in the initial NOA analysis the  $\nu_\mu$  events were not used to constrain the  $\nu_e$  events. This was because a purpose of the first NOA analysis was to address the quality of flux-predictions in an off-axis beam. MiniBooNE has reported that this constraint will be applied in the future.

Figure 2.7 shows the absolutely normalized neutrino energy distribution of  $\nu_\mu$  CCQE events from the NOA line. There is good agreement between data and Monte Carlo. At low energy, the  $\nu_\mu$  data lie somewhat below the Monte Carlo prediction, but well within the systematic error. This is the region where the pion-produced neutrinos dominate. At higher energy, where kaon production dominates the flux, there is good agreement.

The good agreement in the kaon-produced region is important. These kaons also produce the intrinsic  $\nu_e$ s observed in the NOA beam. Thus one expects the prediction of the  $\nu_e$  flux to be good given that the  $\nu_\mu$  distribution from kaons is in agreement. This indicates that using the  $\nu_\mu$  from kaons to constrain the  $\nu_e$  in a later analysis should be successful and reduce the  $\nu_e$  systematic errors, and that the normalization is unlikely to change significantly.

The next step in the analysis constrains the backgrounds and sets the systematic errors, especially on the  $\pi^0$ 's. The MiniBooNE Monte Carlo was in good agreement with NOA  $\pi^0$  data with no re-tuning necessary. The  $\pi^0$  mass peak is shown in Figure 2.8 for events passing likelihood cuts to enhance NC $\pi^0$  events. The agreement is good overall and even in the low invariant mass range. As indicated by the pink histogram, in this range, the data is dominated by the intrinsic  $\nu_e$  distribution. This represents an important cross check before examining the  $\nu_e$  plots, as described further, below.

Figure 2.9 shows the  $E_\nu^{QE}$  distribution for the  $\nu_e$  candidates identified with the same reconstruction and cuts as was used in the BNB analysis. The systematic error on the prediction is large because, in this first iteration, the  $\nu_\mu$  were not used to constrain the  $\nu_e$ . In a future analysis, this error is expected to shrink. At high energy there is good agreement between data and Monte Carlo. At low energy there is systematic disagreement. The significance of the NOA excess is substantially smaller than the BNB excess. There is a  $1.4\sigma$  significance for an excess in the range of 200 to 900 MeV. This is because the  $\nu_\mu$  constraint is not applied and thus the systematics are larger than in the BNB analysis.

Table 2.2 provides complementary information to Table 2.1 on the excess events in the NOA beam.

### 2.1.4 Summary of the Status of the Low Energy Excess

There is an excess of  $\nu_e$  events seen at low energies in the BNB and NOA beams. This excess is significant in the BNB beam, but is only at the  $1.4\sigma$  level in the NOA beam. Continued analysis of the NOA data is underway within MiniBooNE. This will add higher statistics and constrain the  $\nu_e$  with the  $\nu_\mu$ . If the trends persist, then the systematic differences in the excesses may

$E_\nu^{QE}$ [MeV]	200-900	900-3000
total background	401±66	261±50
$\nu_e$ intrinsic	311	231
$\nu_\mu$ induced	90	30
NC $\pi^0$	30	25
NC $\Delta$ rad	14	1
Dirt	35	1
other	11	3
Data	498±22	285±17
Data-MC	97±70	24±53

Table 2.2: Information on the excess observed in the NOA line as a function of two energy bins. Row two shows the total background. Rows three and four divide the backgrounds between intrinsic  $\nu_e$  and Mis-ID. Rows 5 through 8 break out the Mis-ID contributions. Row 9 gives the measurement. Row 10 presents the excess.

provide a clue as to the origin of the events. Assuming that both excesses arise from the same cause, any explanation of the source must confront both data sets.

MiniBooNE has performed extensive cross checks of the BNB data and detector simulation and background prediction. The only significant addition to the background calculation since the excess was first presented is the process of photo-nuclear interactions. This could account for roughly less than 1/3 of the excess seen in the BNB line. Continued analysis and cross checks are under way.

### 2.1.5 Impact of Low Energy Excess on Broader Program

There are a number of models that have been proposed to explain the low energy excess most of which are described in detail in the MicroBooNE proposal. In addition to these, work on more recent ideas has progressed. An interesting example of a new Beyond-Standard-Model explanation is presented in ref. [20]. This model, which introduces a light vector boson with  $(B - L)$  coupling in order to motivate light neutrino masses, fits the MiniBooNE  $\nu$  low energy excess, and predicts a much larger signal in  $\bar{\nu}$  running because of matter effects. This is relevant to this discussion because it can explain why the excess-to- $\nu_\mu$ -CCQE ratio in NOA is much higher than in the BNB beam – it is because of the spectrum of the NOA beam.

There has been continued work on interpreting the signal through anomalous photon production [21]. However, the uncertainty in the normalization of this model translates to accounting for anywhere from 1%-100% of the low energy excess. This model may have difficulty in explaining the angular distribution of the events, though inclusion of nuclear effects may address this. Lastly, it is difficult to see how this model can explain the high excess-to- $\nu_\mu$ -CCQE ratio in the NOA line. Nonetheless, members of the MiniBooNE collaboration are working closely with the authors of this model to include this in the Monte Carlo [22].

Regardless of the interpretation of the excess, for next generation neutrino experiments, the details of the excess must be understood in order to assess the impact on the future neutrino oscillation program. The world-wide neutrino community is embarking on a search for the missing parameter of the 3-neutrino mixing matrix and for evidence of CP violation [23]. A key

component of this program involves searches for  $\nu_\mu \rightarrow \nu_e$  at lower  $\Delta m^2$  than MiniBooNE, but at a similar  $< 1\%$  oscillation probability. To achieve this, the T2K experiment in Japan [24], for example, uses a beam of the same average energy as MiniBooNE and a Cerenkov detector, like MiniBooNE. The T2K oscillation signal is expected to populate the region above 100 MeV. Because of these similarities, depending on the source of the MiniBooNE excess, a background of up to 100 events may appear in the T2K analysis which has not previously been considered. If this background cannot be estimated accurately, this will seriously compromise the T2K program.

If the excess had no  $L/E$  dependence, then in principle a near detector at T2K could address the signal, but in practice the planned near detector cannot, because of its design. About 30 events per year from this effect might be expected in the T2K ND280 near detector. The ND280 is a low tonnage scintillator-strip target, similar to SciBar[25] followed by a TPC which can provide particle identification. Minimum ionizing particles in the few 100 MeV range are indistinguishable until they enter the particle identification region behind the scintillator target. Because of the energy, most of the 30 events expected will not exit the target and will be indistinguishable from the signal. This same design problem has prevented the SciBooNE experiment [26] from addressing the MiniBooNE excess.

It was thought for some time that the low energy excess would not affect the NO $\nu$ A analysis. This was because NO $\nu$ A uses a sharply peaked off-axis beam at 2 GeV, and the reconstructed  $E_\nu^{QE}$  of excess events from the BNB line were at  $< 475$  MeV. However, with the new data from the NOA line indicating a harder excess in a beam with a high energy tail, this assessment must be revisited.

What is needed to measure this potential background for T2K, NO $\nu$ A and other low-probability  $\nu_\mu \rightarrow \nu_e$  searches is a design like MicroBooNE. This design has sufficient baseline to address the question of whether or not there is an  $L/E$  dependence. Also, the detector has the sensitivity to differentiate the signal from backgrounds. These measurements are crucial to the near-term program.

### 2.1.6 Addressing the Low Energy Excess at MicroBooNE

As described in detail in the MicroBooNE proposal, MicroBooNE will be sensitive to the MiniBooNE low energy excess at  $9\sigma$  if the excess is electrons and at  $3.4\sigma$  if it is photons. MicroBooNE will also be exposed to the NOA beam and can, like MiniBooNE, use this as a clue to addressing the low energy excess.

## 2.2 Update on Low Energy Neutrino Cross Sections

The motivation for measurements of neutrino cross sections on argon, both for oscillation physics and as interesting in their own right, is discussed in detail in the MicroBooNE proposal. These measurements will be done using the BNB and the NOA beam from which MicroBooNE will collect  $\sim 100\text{k}$  interactions and  $\sim 60\text{k}$  interactions, respectively.

For the NOA beam, either the LE or ME beam tune can be used for these measurements. There are differences in the shape of the energy spectra, as shown in Figure 2.10. At 250 MeV, the ME flux is reduced by about a factor of 3. At 2 GeV, the ME flux is reduced by about a factor of 2.5. However, in the NOvA era, when it is anticipated that the beam tune will be in the ME mode, there will be a corresponding increase in POT from  $4 \times 10^{20}$  POT per year to  $7 \times 10^{20}$  POT per year. The shape and POT per year differences translate to an additional 30% runtime needed for running in the ME mode. For this reason, the LE mode is preferred, but the ME mode is acceptable.

## 2.3 New: Measurements Relevant to an LAr Proton Decay Detector

Massive detectors will address a range of physics beyond neutrino oscillations including proton decay physics. We expand on the physics case for measurement of neutrino cross sections above to include kinematic measurements in LArTPCs to understand sensitivity to proton decay measurements in LArTPCs.

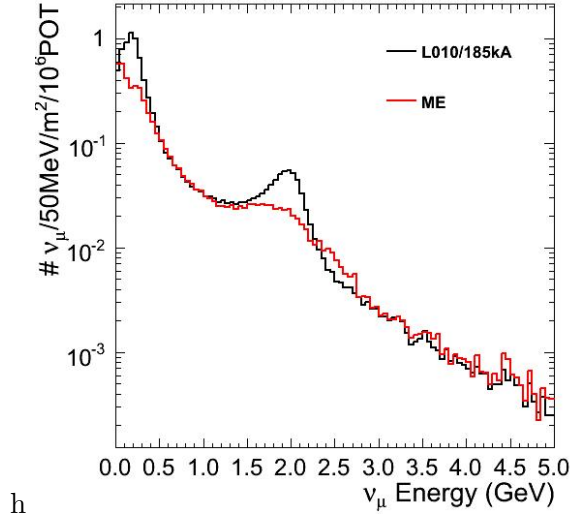


Figure 2.10: LE (black) and ME (red) beam tunes for the NOA beam at the MicroBooNE detector.

K2K has recently published a paper using neutrino induced events in the K2K near detector to understand backgrounds to proton decay searches,  $p \rightarrow e\pi^0$ , in the SuperK detector [27]. This was attempted in MiniBooNE for the proton decay mode  $p \rightarrow \nu k$ , although MiniBooNE’s detection efficiency for kaons made the measurement too difficult. While efficiency in the SciBooNE detector is significantly better, the number of events expected in SciBooNE is too small.

These and other studies show searches in Water Cerenkov (WC) and LArTPC detectors for proton decay mode  $p \rightarrow e\pi^0$  are limited by nuclear absorption of the pion to an efficiency of 45%. By contrast, the efficiency for measurement of proton decay mode  $p \rightarrow \nu k$  in LArTPCs is estimated to be 97%. The efficiency for this decay mode in WC is 14% because the k’s produced are primarily below Cerenkov threshold.

Theory gives no preference to one decay mode over another, hence, LArTPCs add a crucial measurement to this search. While this is very promising, to best estimate LArTPCs sensitivity to this decay mode, actual particle interactions in LArTPCs should be used to measure efficiencies and backgrounds, like in the case of the recent K2K work referenced above. The copious number of neutrino-induced interactions in MicroBooNE provide a nice sample of “signal” k’s

and “background” p’s and  $\mu$ ’s for this measurement. The expected separation in  $dE/dx$  can be tested using MicroBooNE. The number of  $k^+$ ’s expected for this test is  $\sim 480$  events from neutrino induced interactions in the BNB. These numbers assume  $6 \times 10^{20}$  pot from the BNB and 100% detection efficiency. Events from the NOA beam, under study, will also contribute to this physics.

## Chapter 3

# Liquid Argon TPC Research and Development Towards Massive Detectors

Liquid argon detectors show great promise with excellent efficiencies and background rejection for a variety of physics goals. A staged R&D program culminating in the construction of the ICARUS T600 detector [28] has illustrated the capabilities of the technology. However, to develop the technical feasibility of these detectors on the large scales appropriate for long baseline neutrino oscillation physics and proton decay, an aggressive and timely R&D program must be pursued.

For several years there have been efforts growing both in the U.S. and Europe to carry out an R&D plan to address the issues related to large detectors. Small scale test stands have been constructed to address the technical issues and several different large scale detector designs have emerged [5]. These include a modularized detector [29], a single detector but with modularized drift regions [30], and a single open volume, very long drift detector combining charge and light collection [31].

Regardless of the configuration, the major challenges for operating a Liquid Argon detector include:

- achieving and maintaining Argon purity adequate to support electron drift times on the order of 10 msec
- achieving a high signal to noise ratio with readout elements of lengths of up to 10 meters
- optimizing the detector size for constructibility and cost scaling

In recent months, over the course of the Fermilab Project X workshop series, a plan on how to bridge the gap between test stands and the ultimate massive detector has emerged. This plan has been presented recently to HEPAP's P5 committee in a "Golden Book" and in presentations[4, 5].

Detectors ranging in mass from the one ton to one kiloton scale can be deployed in existing Fermilab neutrino beams. Each stage addresses key issues in detector development as well as producing physics results. The shift from R&D to physics evolves with the size of the detector. The R&D goal of the program is to develop a clear concept of how to construct a detector with total mass in the one hundred kiloton range. Along the way timely and exciting physics questions are addressed.

MicroBooNE plays a key role in this program both in studying key R&D questions for the next phase and in prototyping systems to be used for the LAr5 program [32]. In addition, the MicroBooNE detector will be re-used as the near detector for LAr5.

A similar program is emerging in Europe with long range plans to build a massive long baseline LArTPC called MODULAR [33]. The prototype for this program, the SLICE detector, proposes to combine a program of low energy neutrino interaction physics with R&D towards more massive detectors [33]. The MicroBooNE and SLICE collaborations are discussing possible collaborative efforts.

The following sections describes MicroBooNE's R&D program and how this fits into the overall evolving LArTPC program.

### 3.1 Detector R&D

The MicroBooNE R&D program will proceed in two, overlapping phases. The initial R&D phase already underway addresses design questions specific to the MicroBooNE detector. A second R&D phase will address longer term R&D questions relevant for the next stage of LArTPC detectors, the multi-kton scale. There is substantial overlap between these two phases in terms of the issues they address although the timing of each are different. We address R&D questions relevant for the MicroBooNE design in the next chapter. Here we discuss the second R&D phase of the experiment.

MicroBooNE's phase 2, R&D goals are itemized below and described in more detail in the following sections.

- Gain experience with purification and electron drift lifetime in a large system to better understand how best to keep an operating system pure enough. This experience will allow us to define the maximum drift distance for multi-kton detectors.
- Develop low noise electronics suited for the geometry and running conditions of very large detectors. For this, the following issues will be explored:
  - Wire Length: In order to realize the full benefit of the LAr technology, the signal to noise of the readout must be maximized. One critical parameter in the design of large detector is thus the maximum length of the anode wires. The experience we will gain in MicroBooNE both in terms of real measurements and in the analysis of the data will allow us to determine a realistic length that can be used in large detectors.
  - Pre-amps-Cold Electronics: Large LAr detectors will require cold electronics. The MicroBooNE collaboration will use test beds, both in the main detector and in test stands, for new development of cold electronics, building on the experience from Brookhaven National Lab. We have developed a detailed plan starting from hybrid cold preamps, investigating the use of CMOS processes and p-MOS front-end devices for next generation cold preamps.

- For very large detectors where there are potentially  $\sim$ a million channels, the use of cables to bring the signals out to the feedthroughs will not be practical. Thus a method of multiplexing the signal in LAr needs to be developed. There are a number of options including Analog multiplexing and or moving the ADC function into the LAr. Advances in electronics and reduction in power requirements make this possible; however, this does require intensive, well-focused R&D.
- MicroBooNE’s overall design is similar to designs for next generation detectors like LAr5. In particular, aspects of the TPC cage geometry and drift region parameters are likely to be the same or very similar. The overall TPC design including field cage, resistor chain and holders, wire chambers, wire connections and PMT array structure developed on MicroBooNE can be applied to designs for the larger detectors. Value engineering on the MicroBooNE design will directly benefit design work for LAr5 and beyond.
- The MicroBooNE design with its controllable heat shield will allow for studies of the effect of the flow of LAr in the cryostat. These studies will be important for the design for the cooling systems for much larger detectors.

The physics analysis of real data is essential feedback for the above studies. There is no substitute to understanding real issues of signal to noise in the data and understanding of the detector shortcomings and strengths. Thus we see a strong physics program as essential to the R&D.

### 3.1.1 Purification

To date, all LArTPC’s have been evacuated prior to filling with argon. A significant step to demonstrating the feasibility of current designs for multi-kiloton LArTPCs, where for reasons of cost the cryostat is not evacuable, involves achieving clean argon. A major addition to the MicroBooNE R&D program involves just such a test.

Although the MicroBooNE cryostat is designed to be evacuable, we intend to perform this demonstration of achieving clean argon - argon with good electron life-time and good light-

output - without actually evacuating the cryostat. The demonstration will be made the first time we run to ensure that we have not removed contaminants by previous evacuations. If, as expected, we succeed in this demonstration, which includes a fully functional detector inside the cryostat, we will have made a major contribution to the credibility of designs for future multi-kiloton devices.

To achieve a drift lifetime of 10 milliseconds requires an oxygen-equivalent concentration of 30 parts per trillion (ppt) in liquid or of 25 parts per billion (ppb) in the gas which mixes with pure liquid. The process for removing the atmosphere in the cryostat begins with purging with gaseous argon to reduce the oxygen concentration to a few ppm. Perfect mixing would require about 10 volume changes to reduce the oxygen concentration in the cryostat to 10 ppm; tests at Fermilab have demonstrated that if one exploits the fact that argon is heavier than air and introduces the argon carefully at the bottom of a tank, the number of volume changes required is about half as many [34]. In either case, this process is neither costly nor time-consuming and it is easy to measure the actual concentration. Purging of a similar horizontal tank, the RICH detector of the SELEX (FNAL E-781), experiment is described in [35].

Once the oxygen concentration is at the 10 ppm level, there are two possible options. The gas can be recirculated as gas through a standard purifier; tests at Fermilab using a small oxysorb filter have achieved levels below 1 ppb oxygen concentration in an industrial vessel. Alternatively a small amount of liquid argon can be introduced into the tank and recirculated through the filtration system <sup>1</sup>.

The requirements on nitrogen contamination are, fortunately, much less severe than those on oxygen. Nitrogen even at several ppm, does not affect the electron drift-lifetime [36]. The more stringent criterion comes from the light output which is affected by levels of nitrogen above 1 ppm [37]. This criterion is met by the initial purging which reduces the nitrogen

---

<sup>1</sup>This process is more efficient than the simple mass ratios of the liquid to gaseous argon would imply. Because oxygen has a higher boiling point than argon, the oxygen will be more concentrated in the liquid than in the gas (the liquid-to-gas concentration ratio is about 3 to 1). Given that the liquid to gas density ratio of argon is 850, filling 1% of the cryostat volume will reduce the oxygen concentration by a factor of  $8.5 \times 3 \approx 25$ . Two such fillings should reduce the 10 ppm oxygen concentration by a factor of 625, i.e. to 16 ppb.

contamination to  $\approx 40\text{ppm}$  in the gas producing  $\approx 50\text{ppb}$  in the liquid, well below the level where the light output is believed to be affected.

Filters to remove water vapor will operate continuously since water will be released by the walls of the vessel and the materials of the TPC as long as the tank is warm. We are investigating the usefulness of heating the circulating gas and/or the vessel.

We expect the process from atmosphere to usable argon to take about a month and have reserved 6 weeks for this process in our schedule. This schedule presents a minimal delay to MicroBooNE's physics program.

### 3.1.2 Readout Electronics

A rigorous R&D program to develop integrated electronics is an essential key for the success of future very large LAr detectors for neutrino experiments. The MicroBooNE program addresses the two main questions for large detectors:

- A massive detector ( $>5\text{kton}$ ) may require  $\sim$ a million readout channels. The number of services, feedthroughs and cabling has to be optimized. Foreseeable readout architecture will be likely based on an integrated ASIC design that includes one or more multiplexing levels and operating at cryogenics temperatures.
- To optimize the detector performance (maximum signal-to-noise ratio) and decouple readout aspects from detector layout and geometry, the readout ASIC should operate optimally at LAr temperature.

The MicroBooNE baseline design addresses the question of optimal performance of the analog front-end at cryogenic temperatures. The pre-amplifier circuit is realized through discrete JFET hybrids, which have been successfully designed at BNL and used in LAr and LKr calorimeters in several past experiments (e.g Helios, NA48, ICARUS). The optimal noise performance is attained at 120K (please see Fig. 4.45 on page 101 of the proposal). The Pre-amplifiers, therefore, will be housed on PC boards in the Ar gas volume inside the vessel, at this optimal

temperature. The noise levels degrade by about 30% at LAr temperature (87K) using this technology. For the steps beyond MicroBooNE where geometry dictates the need for pre-amplifiers in LAr, a newer technology is being explored within the phase 2 R&D program.

Specifically, large scale integration, mixed analog/digital functionality design, motivates the use of CMOS technologies. CMOS devices, the main staple of modern integrated electronics, are capable of cryogenic operations. Preliminary tests conducted at BNL on a commercially available CMOS process cooling devices down to LHe temperature [38] shows that both NMOS and PMOS devices were working at 77K, and subsequent failures approaching 4K were attributable to excessive thermal stresses which caused rupture of metal lines.

MOS devices still have a much larger  $1/f$  noise than JFETs, but, thanks to modern process technology, they have a larger  $g_m$  when operated at comparable currents. NMOS devices have too much  $1/f$  noise for the shaping time used in LArTPC detectors, but PMOS devices look attractive for readout of large capacitance detectors at LAr temperature.

For example a large PMOS in a quarter-micron CMOS process with  $W=60\mu\text{m}$  at a current of 10mA, is simulated to show a low  $e_n=0.25\text{nV}/\sqrt{\text{Hz}}$  and a capacitance  $C_{ISS}=116\text{pF}$ , and a still acceptable  $1/f$  noise, based on noise data measured at room temperature.

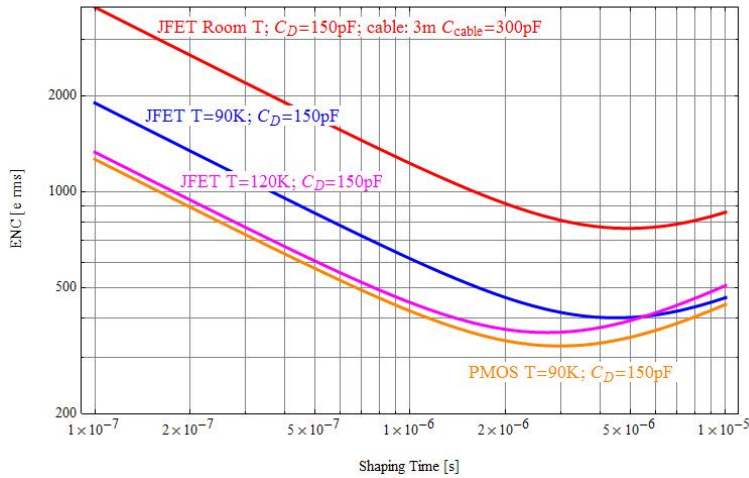


Figure 3.1: Comparison of ENC(noise-to-signal ratio) for JFET devices in different conditions and for PMOS monolithically integrated transistors.

For comparison a JFET of similar capacitance would have an  $e_n=0.4\text{nV}/\text{Sqrt}(\text{Hz})$ . Figure 3.1 shows the predicted ENC when used for the readout of MicroBooNE.

We are planning a feasibility study of a readout architecture based on front-end CMOS ASICs. The research would proceed in three phases:

- Characterization of the most recent ASIC developments at very low temperature, including signal and noise performance of analog and digital sections as well as power considerations.
- Readout architecture studies addressing specific functionality aspects such as multiplexing, digitization and data transmission, evaluating pros and cons of different schemes and understanding the impact of these schemes on the detector performance.
- Development and design of an ASIC for this application, with amount of integrated functionality, which will depend on the results from the previous phases.

What is learned from this electronics R&D work is a key piece in design for future large LAr detectors.

## 3.2 Physics R&D

Research and Development towards realizing these large detectors in the U.S. has been hampered by the lack of a real proof of principle experiment using this technology to do a forefront neutrino measurement. The MicroBooNE physics case is specifically motivated by addressing the MiniBooNE low energy excess as described in Chapter 2 and measuring neutrino cross sections. The impact of using this technology for a physics measurement should not be underestimated. In particular, the development of tools for physics analyses and measurements of neutrino cross sections add a crucial piece to the evolution of the LArTPC detector program.

### 3.2.1 Physics Development

The MicroBooNE proposal describes the need for measuring efficiencies and purities for  $\sim 1$  GeV neutrino interactions on Argon for next generation neutrino experiments. In addition, the need for measuring neutrino cross sections, both for oscillation physics and as interesting in their own right, is discussed in the proposal and in Chapter 2. Newly described here is the motivation for measuring kinematics of kaon production to understand sensitivity to Proton Decay measurements. This is presented in Chapter 2.

### 3.2.2 Analysis Tools

Although LArTPC R&D has been ongoing for almost 20 years, primarily in Europe and more recently in the U.S., no fully automated reconstruction package exists for these detectors. The only published neutrino interactions in an LArTPC detector [39], the 50 liter ICARUS prototype exposed to the NOMAD beam, uses a combination of automated techniques and hand-scanning to analyze events.

For experiments such as MicroBooNE and beyond which will collect more than a hundred thousand events, fully automated reconstruction techniques must be developed.

In addition to reconstruction techniques, simulation and data analysis techniques need to be developed, fine-tuned, and tested using real data. Without a full experimental test such as MicroBooNE, these techniques are unlikely to be fully explored.

## Chapter 4

# Baseline Design Update

Following the recommendations of the PAC to the proposal submitted in October 2007 we have made a systematic review of the proposal to address two main issues raised by the PAC and FNAL management.

- Review the design to minimize cost.
- Address the R&D implementation issues for MicroBooNE to make sure they will be relevant to large LAr detectors needed for the next generation of neutrino experiments.

As a result of these considerations, we have made significant changes to the design of the Cryostat and the Cryogenic system. The main design change was to move from a double wall vessel with vacuum insulation to a foam insulated single vessel Cryostat that will reduce cost significantly. This change allows the use of single warm flange sealing feedthroughs that are similar to those employed in large volume cryogenic vessels. An overview picture of the new design is depicted in Figure 4.1. Costs were further optimized by removing the large LAr storage Dewar from the system by using the LAr volume for neutrino detection and for liquid storage.

An additional change was made to drive the pre-amp output signals using twisted pair transmission lines. This is mostly a cost optimization due to the high cost of the Kapton mini-coaxial cable in the original design. We have introduced a small faraday cage with cable

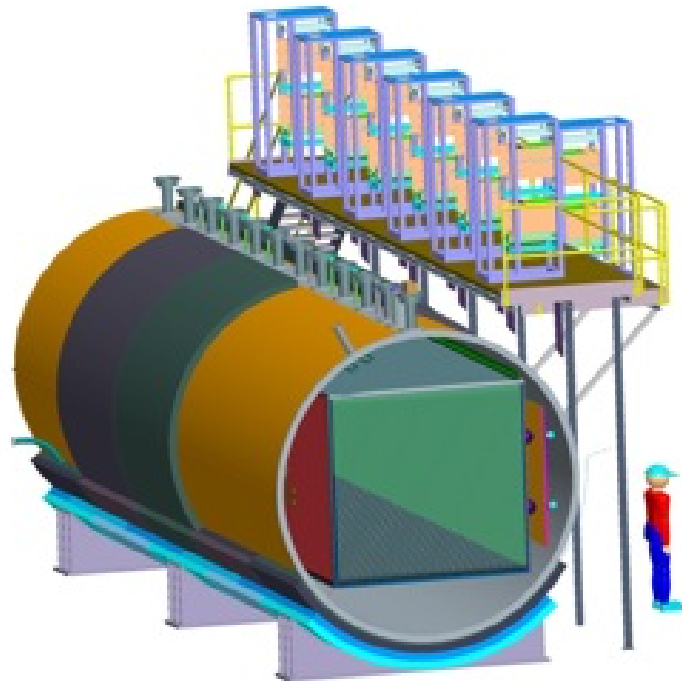


Figure 4.1: Single vessel design with multi-layered insulation.

drivers on the top of the feedthroughs. This will enable location of the readout electronics close to the detector but not necessarily right at the feedthrough location. The change is partially motivated by being closer to a system that can be extrapolated to a large system.

Significant progress has been made in refining the design of the experiment. Prototypes of preamps have been built, the readout chain has been established, and Cryostat design has progressed. By completing this detailed design work and related tests now, we anticipate reducing the time scheduled for design work in the future.

In the following we give a summary of the main changes to the design.

## 4.1 Cryostat and Cryogenics

In the time since the November '07 PAC meeting we have carried out a detailed study of three different cryostat designs to determine which approach would minimize construction costs while

providing all necessary operating conditions for a LArTPC wire detector. The three designs studied include a standard cryostat with double walls and vacuum insulation. The second design has a similar cold vessel but with mechanical insulation replacing the outer vessel and vacuum insulation. And third a mechanically insulated rectangular vessel having flat walls. The second and third types are both mechanically insulated as are the very large kiloton volume cryogenic tanks. Though their volumes differ greatly, design for management of heat loads, feedthroughs, cooling etc. are very similar.

In addition, the question of reducing the cold vessel wall thickness from 1 inch, with the ability to pump and purge, to a thickness of 0.5 inch where only purging is possible was also looked at in some detail. Pros and cons were discussed and the decision was, that for a 10% cost difference, we choose to go with the heavier wall to have the ability to both pump and purge. This feature gives us the flexibility to both perform the purification purge tests described in detail in Chapter 3, a crucial piece of MicroBooNE's R&D program, while maintaining the flexibility to evacuate if necessary, following the purge test.

#### 4.1.1 Cryostat

The first design, a so called standard cryostat, was fully explained in the MicroBooNE Proposal. This design with a warm and cold vessel, vacuum insulated is reliable, has the lowest heat leak and usually is the most expensive.

The third option, the rectangular design, was originally imagined to have some advantages, such as more efficient use of the LAr volume, lower construction cost and easier installation of mechanical insulation as opposed to a cylindrical vessel. But upon further study of the design, these advantages vanished. It was found, for example, that the increase in useful volume of LAr was minimal because of space allocated for high voltage and photomultiplier tubes. In addition, it was found that the flat vessel walls needed lots of reinforcement which increased costs but also made installation of mechanical insulation more difficult and costly.

The second option of a single-walled, mechanically insulated, cylindrical vessel is Spartan but preserves important operating parameters and detection quality. With this design, con-

struction costs are reduced by \$335,000 however, the yearly LN2 operating costs increase by 220% (\$76k vs. \$34.3K). This difference arises from a decrease in the insulation efficiency of the mechanical foams compared to vacuum insulation. Calculations show that heat leak for the entire surface area of the detector through 12 inches of foam totals 3400W. However, the interior detecting liquid should be as isothermal and free of convection as possible to minimize track distortion. To isolate the detector LAr from the heat leak through the foam, a temperature controlled copper shroud will be placed around the surface of the cold vessel to intercept this heat before it reaches the active volume of the detector. By adjusting the shroud and internal sub-cooling loop temperatures, the effect of the external heat can be eliminated. The technique of a thermal shroud intercept for foam heat leak is directly transferable to kiloton designs.

An interesting secondary benefit of a foamed vessel is that the foam can be used in a cradle design to support the fully loaded vessel of 220 tons. In this use, foam has another advantage in that inner vessel support legs or slings are not needed thus reducing complexity and heat leak, all adding up to reduced cost. This design, the foam insulated cylindrical cold vessel, has the best combination of technical advantages, lowest cost and designs directly applicable to tomorrow's kiloton detectors.

#### 4.1.2 Feedthroughs

Details of feedthrough designs differ between vacuum and foam insulated cryostats. The foam insulated type is simpler and less expensive because one warm sealing flange will provide a workable feedthrough but one of higher heat load. However, the warm feedthrough must be positioned in such a way that liquid cryogen will not enter the cold to warm transfer tube. In the case of our detector, feedthrough heat loads equal  $\sim 500$  Watts which when added to cold electronics dissipation and other miscellaneous sources total over 2kW.

Figure 4.2 is a cross section of the foamed detector showing a typical warm feedthrough penetrating the gas buffer volume at the top of the vessel. Many warm feedthroughs will be placed on top over the length of the vessel to bring both electrical and mechanical services to the outside. Heat leaks will be neutralized and detector internal pressure stabilized by re-

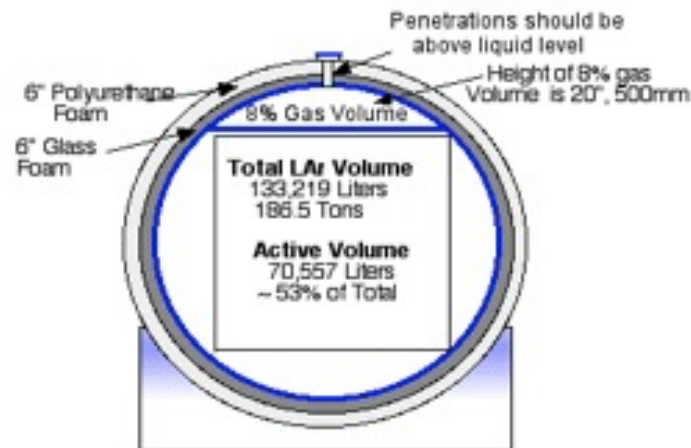


Figure 4.2: Cross Section of the Detector showing a typical warm feedthrough penetrating the Foam insulating layers.

condensing heat exchangers in the gas buffer volume. The design and use of warm feedthroughs in this application is 100% transferable for use in very large kiloton detectors.

## 4.2 TPC Detectors: Wires, HV, and Drifting Field

### 4.2.1 High Voltage and Drifting Field

To avoid the high electric field in the gas volume above the liquid level near the HV side of the detector, a grounded conductor plane slightly below the gas-liquid interface is added. This plane will contain the electric field from the drift electrodes and minimize the electric field in the gas phase. Figure 4.3 shows the distribution of the field strength in the top half of the TPC cryostat, with an ullage of about 8%.

### 4.2.2 Wire Termination

We have developed a technique for terminating the wires. The wires will be terminated by wrapping around brass rings with grooves, very similar to the ICARUS design. This solution

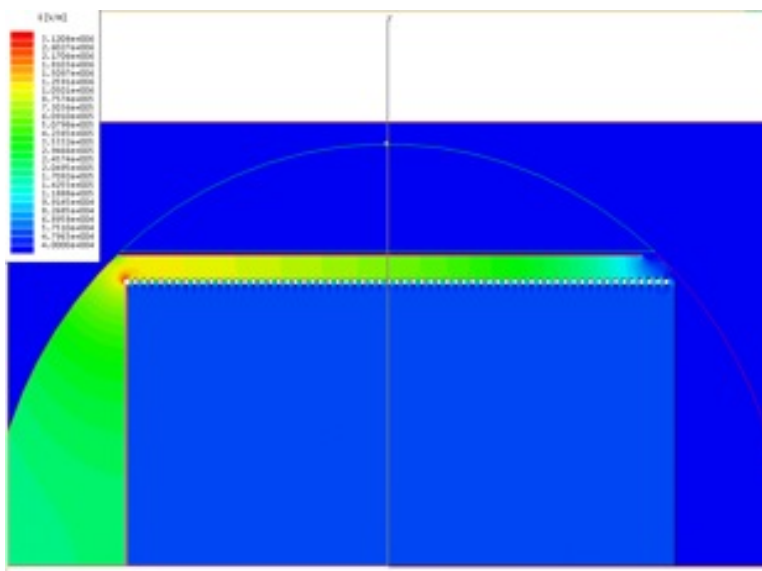


Figure 4.3: Electric Field Map at the liquid-gas interface and additional ground plane to limit the electric field in the gas.

prevents “creeping issues” observed during wire termination tests, when crimped terminations are not steadfast. The brass rings are about 3mm OD, 1.5mm thick. These rings with wire attached will be captured by the cavities in the wire holder. Tests have shown that such wire termination can withstand wire tension up to 3kg, using  $150\mu\text{m}$  SS304V wire. Figure 4.4 shows a photograph of the new termination scheme.

We are in the process of designing and building a winding machine to study and optimize the wire termination procedure. Figure 4.5 depicts a sketch of the mechanical fixture that will hold the brass ring in place allowing the wire to be wrapped around it.

### 4.2.3 Wire Mechanical Properties Comparison

Mechanical studies of wire samples at room and LN2 temperature were conducted. The baseline design specifies wires to be gold plated SS304  $150\mu\text{m}$  diameter. Manufacturing and plating are two separate processes with potential cost impact. Alternatively a CuBe ( $\text{OD} = 150\mu\text{m}$ ) wire has been considered to achieve comparable DC resistances with less impact on cost. Figure 4.6 summarizes the main conclusions from several mechanical measurements. Ultimately the deci-

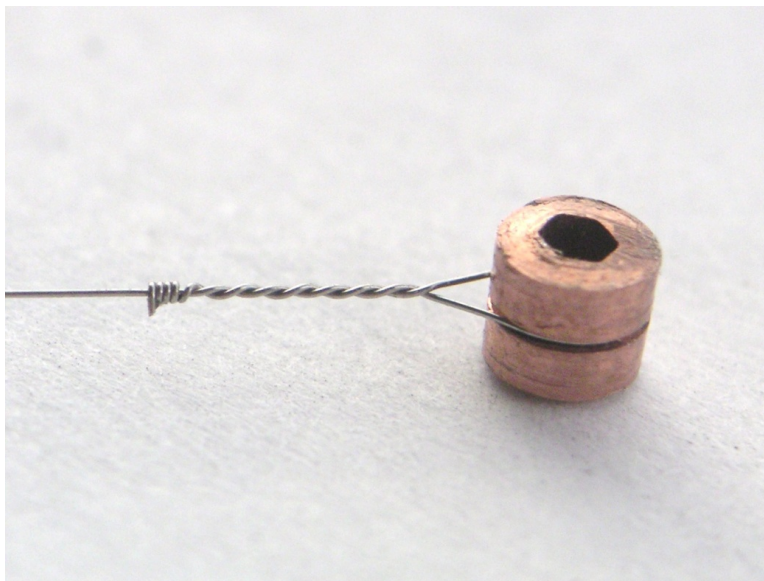


Figure 4.4: Photograph of the new wire termination scheme.

sion of using SS304 gold plated wires has been confirmed given the better margin in tensioning the wires.

### 4.3 Readout Electronics and DAQ

The readout electronics configuration has been rearranged to improve rejection of electromagnetic interference and increase flexibility in the location of the high-power DAQ portion of the readout chain. The use of a foam-insulated cryostat and warm feedthrough reduces the number of connectors necessary for the cold-to-warm transition, and allows the use of less expensive and easier to terminate twisted pair cable for the connections. The pre-amplifier will still have a single-ended driver (to reduce power), but it will drive pseudo-differentially (i.e. the second conductor of the pair will be terminated to ground with the proper characteristic impedance). Such connection requires two cryostat penetrations per channel, but allows the use of a fully differential receiver to partially cancel cable pickup interference.

To preserve the integrity of the cryostat Faraday cage and allow the positioning of the DAQ racks farther away from the detector, a differential line receiver and differential driver/amplifier have been added in a crate, which is an integral part of the cryostat Faraday cage. This

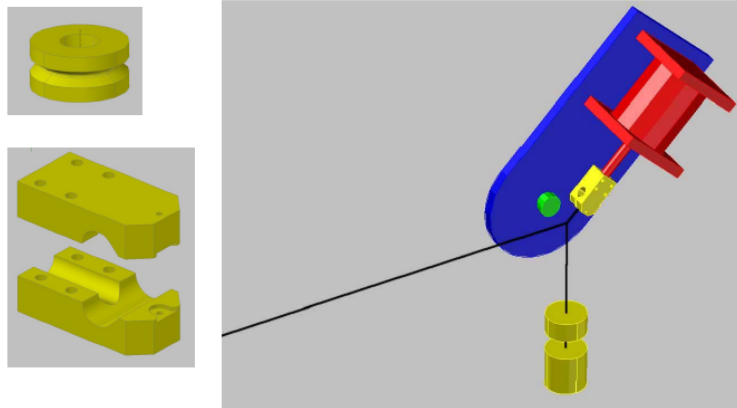


Figure 4.5: Sketch of a possible winding machine design.

will improve rejection of electromagnetic interference (EMI) and will allow driving of a longer differential pair to the DAQ electronics, which can thus be sited in a more convenient location farther away from the cryostat.

Figure 4.7 (an updated version of Figure 4.46 on page 103 of the proposal) is a schematic showing the changes in the readout chain. The pre-amplifier output signals are driven pseudo-differentially to a single warm feedthrough flange and amplified by an intermediate, fixed gain amplifier installed on the top of the feedthrough pin carriers in a dedicated faraday cage. Individually shielded twisted pair transmission lines will drive the signal to the DAQ crates. The advantages will be twofold:

- Easier cable assembly particularly for the termination at the feedthrough ends. The mini-coaxial design terminated by ATI-64 pin connector has proven to not be a cost effective solution.
- Possibility of driving the signals at a larger distance allowing for locating the DAQ racks at a more convenient position, likely in the MiniBooNE near detector hall.

The pre-amplifier design has been optimized and repackaged ex-novo to reduce the manufacturing costs. Individual hybrids using ceramic substrate and screen printed resistors have been replaced with a four channel design using ceramic based printed circuit technology and SMD resistors. A few prototypes have been manufactured and are currently under evaluation

### Update on SS304 and CuBe wire properties

	SS304V (Fort Wayne)	CuBe (Little Falls Alloy)
Young's modulus @ RT	170GPa	121GPa
Young's modulus @ LN2	183GPa (8% increase)	136GPa (12% increase)
Integral CTE	0.22%	0.29%
Tension increase due to cooling	~750g	~730g
Max. tension with termination	~3kg	~2kg

Figure 4.6: Wire property comparison chart

in a test setup at Brookhaven. A full characterization (noise, gain, linearity, dynamic range at cryogenic temperatures) and measurement results will be available for the PAC presentation. Figure 4.8 is a photograph of the hybrid prototype.

Figure 4.9 shows a 3D-model of the interconnections between the wire-holders mounted on the support frame and the motherboard PCBs housing the pre-amplifier hybrids.

To further reduce costs, the DAQ board design has been revised as well. The architecture is the same as the one described in the original proposal. The boards however will be assembled in 1U hermetic cases, rack mounted – not in a standard communication crate (e.g. VME or ATCA).

A demonstration project to validate the full readout and DAQ architecture is well underway. The FPGA algorithms, the DDR2 pipeline, the ADC interface as well as the G-bit Ethernet interface are being bench-tested through demonstration boards by Xilinx. A custom adaptor board allows testing of the communication between the Analog Devices ADCs and the Xilinx FPGA. Figure 4.10 is a picture of the setup used during preliminary tests at Brookhaven. A prototype board has been laid out and submitted for fabrication and is expected to be ready and assembled by early March.

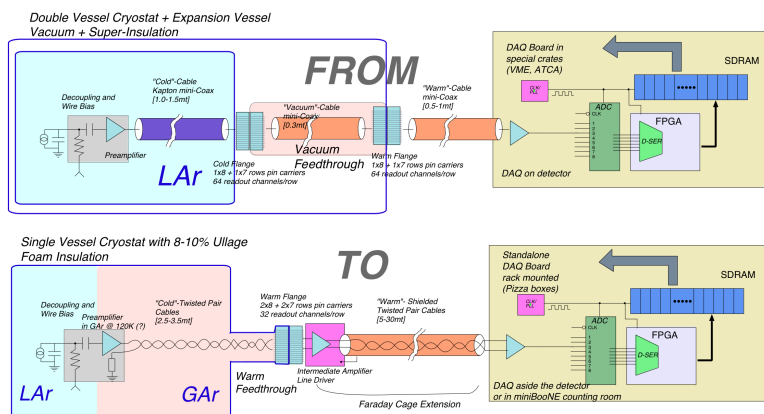


Figure 4.7: Single Channel Readout design changes. A comparison between the baseline design described in the proposal and the newer, more economical, version

## 4.4 Summary

The baseline design has been re-evaluated in light of R&D and cost considerations and updated accordingly. The main changes are to the cryostat and readout electronics, as described here.

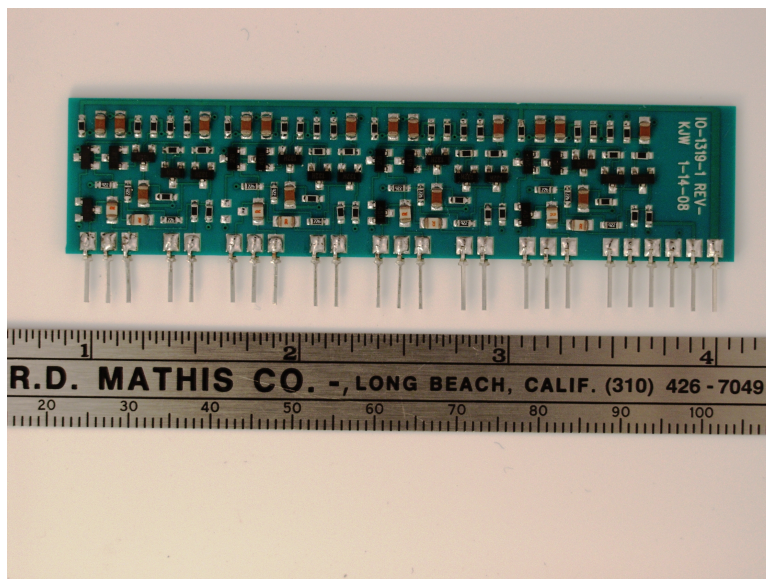


Figure 4.8: First discrete quad-channel pre-amplifier prototype for MicroBooNE.

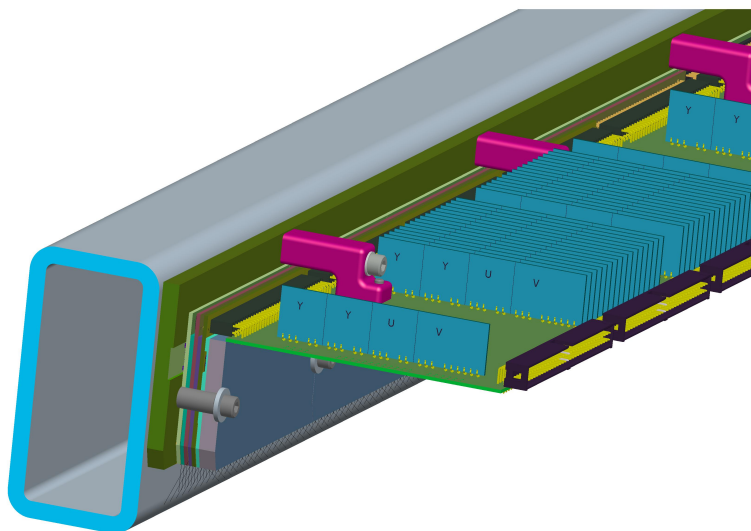


Figure 4.9: Wire-holder, pre-amplifier hybrids and motherboards. 3D model of the overall assembly.

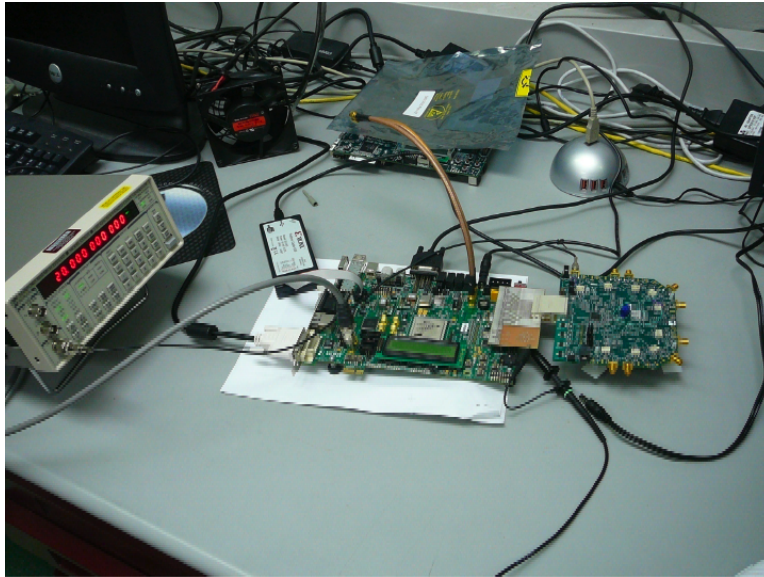


Figure 4.10: DAQ demonstrator setup.

## Chapter 5

# Overview of MicroBooNE Cost, Schedule, and Siting

Modifications to the baseline design were guided by MicroBooNE's R&D goals as described in Chapters 3 and 4, including value engineering both for MicroBooNE and for the steps beyond. As a result, costs for the cryostat and cryogenics, in particular, have been optimized. Costs for the electronics, and detector systems have also been updated. The tables below in Figures 5.1, 5.2, 5.3, and 5.4 outline the major costs for the experiment and separately for the major systems. A much more detailed cost estimate is posted here [6].

Work on the schedule, in conjunction with the Fermilab directorate, is in progress. The status of the schedule will be presented at the time of the PAC presentations. Costs for labor will increase if the schedule is stretched.

Work on siting of the detector enclosure has progressed. Figure 5.5 shows the MicroBooNE enclosure on the BNB beam axis just upstream of the MiniBooNE detector. A hard line is shown from the MicroBooNE detector to the MiniBooNE detector hall, where the MicroBooNE off-detector electronics can be housed. The MicroBooNE enclosure has been estimated by Fermilab's FESS division to be \$295,000, and is described in reference [40]. This cost is included in the tables below.

Oxygen Deficiency Hazard (ODH) considerations are being studied for MicroBooNE in

	Total Cost Estimate	Labor Cost Estimate	Materials Cost Estimate
<b>MicroBooNE costs</b>	\$15,583,500.00	\$6,645,000.00	\$8,938,500.00
Contingency 50% of summed estimates	\$5,194,500.00	\$2,215,000.00	\$2,979,500.00
Sum of Estimates listed below	\$10,389,000.00	\$4,430,000.00	\$5,959,000.00
Facility and Infrastructure	\$425,000.00	\$0.00	\$425,000.00
Cryostat, Cryogenics, and Feed-throughs	\$4,457,000.00	\$1,695,000.00	\$2,762,000.00
Detector - TPC and Photodetector	\$1,110,000.00	\$480,000.00	\$630,000.00
Electronics, Readout, and Power Supplies	\$2,887,000.00	\$1,145,000.00	\$1,742,000.00
DAQ & Monitoring	\$310,000.00	\$110,000.00	\$200,000.00
Installation, Integration, and Commissioning	\$1,200,000.00	\$1,000,000.00	\$200,000.00

Figure 5.1: Cost Estimate for the MicroBooNE Detector.

this surface location. Fermilab has standard requirements for evaluating the potential Oxygen Deficiency Hazards (ODH) that are spelled out in Fermilab Environment, Safety and Health (FESHM) chapter 5064. The MicroBooNE design will be analyzed to determine failure and leak rates for all components of the cryogenic system. This analysis determines the severity of the hazard. Training, procedures and safety equipment needed will then be defined according to mitigation requirements in the FESHM chapter 5064.

The analysis will be done in conjunction with the cryogenic system design to reduce the hazard and keep costs reasonable. Results should be comparable with other large argon detectors on Fermilab site, such as E706 and Dzero.

MicroBooNE	Total Cost Estimate	Labor Cost Estimate	Materials Cost Estimate	Material & Labor Resource Items
<b>Cryostat, Cryogenics, and Feed-Throughs</b>	<b>\$4,457,000.00</b>	<b>\$1,695,000.00</b>	<b>\$2,762,000.00</b>	
Cryostat Vessel	\$1,265,000.00	\$465,000.00	\$800,000.00	Cryostat Vessel Material & Assembly Labor Cryostat Engineer/Design Labor
Cryostat Insulation	\$250,000.00	\$180,000.00	\$70,000.00	Vessel Insulation Material & Labor
LAr Cryogenics System	\$1,100,000.00	\$550,000.00	\$550,000.00	LAr Purification & Recirculation, Cryo Controls, LAr Cryo system feed-throughs
Cryogenics Vacuum System	\$130,000.00	\$0.00	\$130,000.00	
LN2 Cryogenics System	\$1,400,000.00	\$300,000.00	\$1,100,000.00	LN2 Plumbing, valves, parts; LN2 pumps, LN2 Dewar, LN2 assembly labor
Detector (TPC & PM) Feed-through	\$312,000.00	\$200,000.00	\$112,000.00	TPC Signal FT flanges (12), TPC HV FT flange, PM Signal FT, PM HV FT, Signal and HV FT Assembly labor

Figure 5.2: Cost breakdown for the cryogenics and purification systems, not including contingency.

MicroBooNE	Total Cost Estimate	Labor Cost Estimate	Materials Cost Estimate	Material & Labor Resource Items
<b>Detector - TPC and Photodetector</b>	<b>\$1,110,000.00</b>	<b>\$480,000.00</b>	<b>\$630,000.00</b>	
Signal wire planes estimate	\$360,000.00	\$150,000.00	\$210,000.00	TPC wire plane assembly, signal wire, wire plane winding machine, wire holders and drums, wire carrier and frames, wire winding labor
Field cage estimate	\$440,000.00	\$200,000.00	\$240,000.00	Field Cage cathode plane, Cage design and assembly labor, Cage tubing, Cage frame, resistors and holders
TPC Mechanical Support	\$100,000.00	\$50,000.00	\$50,000.00	TPC support attachments
PMTs & bases	\$110,000.00	\$30,000.00	\$80,000.00	Photomultiplier Detectors, PM assembly and testing
PMT Mechanical Support	\$100,000.00	\$50,000.00	\$50,000.00	PM support attachments

Figure 5.3: Cost breakdown for the detector systems, not including contingency.

MicroBooNE	Total Cost Estimate	Labor Cost Estimate	Materials Cost Estimate	Material & Labor Resource Items
Electronics, Readout, and Power Supplies	\$2,887,000.00	\$1,145,000.00	\$1,742,000.00	
TPC on-detector electronics	\$250,000.00	\$100,000.00	\$150,000.00	TPC Pre-Amp & Drivers
TPC off-detector electronics	\$2,305,000.00	\$920,000.00	\$1,385,000.00	TPC Readout Electronics, Signal Cables, Calibration Cables
TPC electronics LV Power Supply	\$87,000.00	\$35,000.00	\$52,000.00	Pre-Amp power cables, Electronics LVPS, LVPS assembly and testing labor
TPC HV Power Supply	\$85,000.00	\$50,000.00	\$35,000.00	TPC HV PS, TPC HV cables, HV cable assembly and testing
Photomultiplier Detector readout	\$45,000.00	\$15,000.00	\$30,000.00	PM digitizer & readout, PM readout cables
PM HV Power Supply	\$35,000.00	\$15,000.00	\$20,000.00	PM HV PS, PM HV cables
Racks	\$170,000.00	\$100,000.00	\$70,000.00	Racks & readout support
DAQ & Monitoring	\$310,000.00	\$110,000.00	\$200,000.00	
DAQ estimate	\$250,000.00	\$100,000.00	\$150,000.00	DAQ Hardware & labor
Monitoring estimate	\$60,000.00	\$10,000.00	\$50,000.00	Detector Monitoring Hardware & labor
Installation	\$1,200,000.00	\$1,000,000.00	\$200,000.00	Installation labor & materials

Figure 5.4: Cost breakdown for the readout electronics and DAQ, not including contingency.

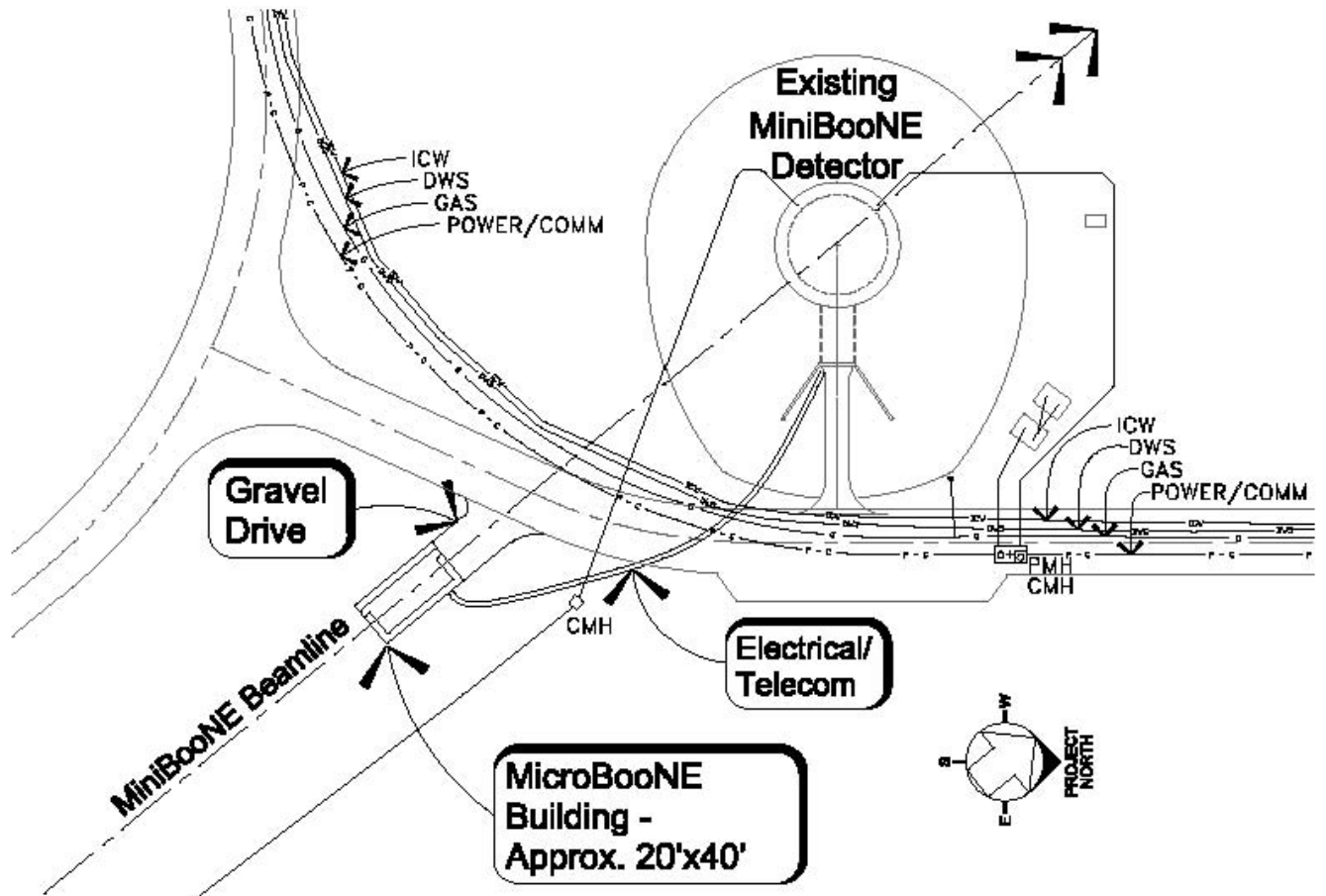


Figure 5.5: MicroBooNE enclosure shown on beam axis just upstream of the MiniBooNE detector.

## Chapter 6

# Conclusions

The MicroBooNE experiment is proposed to address the low energy excess observed by the MiniBooNE experiment, measure low energy neutrino cross sections on argon, and serve as the next necessary step the R&D path towards multi-kiloton LArTPC detectors. This addendum to the MicroBooNE proposal describes the following:

- The status of the MiniBooNE low energy excess, in particular, clarification of the signal and backgrounds and new results from events from the NuMI beam.
- Study of kinematics of kaons in LArTPCs towards characterizing the signal for proton decay,  $p \rightarrow \nu k$ .
- An expanded R&D program to include the issues relevant to multi-kiloton LArTPCs. MicroBooNE is the next necessary step in the optimal evolution of LArTPCs in the US program as has been studied recently in the Project X workshop series.

MicroBooNE is a timely experiment addressing a combination of physics and R&D goals. It will both resolve the low energy excess observed by MiniBooNE, a key issue for next generation neutrino oscillation experiments, and advance R&D towards multi-kiloton LArTPCs, potentially a future flagship program in US neutrino physics.

# Bibliography

- [1] H. Chen *et al.*, “A Proposal for a New Experiment Using the Booster and NuMI Neutrino Beamlines: MicroBooNE”, submitted to the Fermilab PAC, Fall 2007.
- [2] Deep Underground Science and Engineering Laboratory, <http://www.int.washington.edu/DUSEL/>
- [3] The Fermilab Project X Workshop Series, [http://www.fnal.gov/directorate/Longrange/Steering\\_Public/workshop\\_physics.html](http://www.fnal.gov/directorate/Longrange/Steering_Public/workshop_physics.html)
- [4] ”Physics with a High Intensity Proton Source at Fermilab”, [http://www.fnal.gov/directorate/Longrange/Steering\\_Public/P5.html](http://www.fnal.gov/directorate/Longrange/Steering_Public/P5.html)
- [5] See presentations to the DOE/NSF P5 Committee, <http://hepwww.physics.yale.edu/P5/>
- [6] <http://www-microboone.fnal.gov>
- [7] A. A. Aguilar-Arevalo *et al.* [The MiniBooNE Collaboration], Phys. Rev. Lett. **98**, 231801 (2007) [arXiv:0704.1500 [hep-ex]].
- [8] Joint Theoretical-Experimental Seminar presented by Z. Pavlovic and Z. Djurcic, Dec. 11, 2007, Fermilab. Slides available from the MiniBooNE webpage: <http://www-microboone.fnal.gov>.
- [9] D. Casper, Nucl. Phys. Proc. Suppl. **112**, 161 (2002).
- [10] A. A. Aguilar-Arevalo *et al.* [MiniBooNE Collaboration], arXiv:0706.0926 [hep-ex].
- [11] CERN Program Library Long Writeup W5013 (1993).

- [12] C. Zeitnitz and T.A. Gabriel, Nucl. Instrum. Meth. **A349**, 106 (1994).
- [13] B.C. Brown *et al.*, IEEE Nuclear Science Symposium Conference Record 1, 652 (2004).
- [14] R. B. Patterson, “A search for muon neutrino to electron neutrino oscillations at  $\delta(m^2) > 0.1 \text{ eV}^2$ ,” CITATION = FERMILAB-THESIS-2007-19;
- [15] Talk presented by Rex Tayloe at Lepton Photon '07. <http://chep.knu.ac.kr/LP07/>
- [16] This figure is from M. Shaevitz's talk at TAUP'07.Slides available from the MiniBooNE webpage: <http://www-boone.fnal.gov>.
- [17] See <http://www-boone.fnal.gov>
- [18] MiniBooNE paper in preparation
- [19] J. R. Monroe, “A combined  $\nu/\mu$  and  $\nu/e$  oscillation search at MiniBooNE,”, CITATION = FERMILAB-THESIS-2006-44;
- [20] A. E. Nelson and J. Walsh, “Short Baseline Neutrino Oscillations and a New Light Gauge Boson,” arXiv:0711.1363 [hep-ph].
- [21] J. A. Harvey, C. T. Hill and R. J. Hill, 0708.1334 [hep-ph].
- [22] Van Nguyen, Private communication
- [23] “Joint Study on the Future of Neutrino Physics” The APS neutrino study, 2004.
- [24] <http://jnusrv01.kek.jp/public/t2k/>
- [25] <http://neutrino.kek.jp/>
- [26] A. A. Aguilar-Arevalo *et al.* [SciBooNE Collaboration], “Bringing the SciBar detector to the booster neutrino beam,” arXiv:hep-ex/0601022. HEP-EX/0601022;
- [27] S. Mine *et al.* [K2K Collaboration], “Experimental study of the atmospheric neutrino backgrounds for proton decay to positron and neutral pion searches in water Cherenkov detectors,” arXiv:0801.0182 [hep-ex].

- [28] S. Amerio *et al.* [ICARUS Collaboration], “Design, construction and tests of the ICARUS T600 detector,” Nucl. Instrum. Meth. A **527**, 329 (2004).
- [29] D. B. Cline, F. Raffaelli and F. Sergiampietri, “LANNDD: A line of liquid argon TPC detectors scalable in mass from 200-tons to 100-ktons,” JINST **1**, T09001 (2006) [arXiv:astro-ph/0604548].
- [30] ”Recommendations to the Department of Energy and the National Science Foundation on a Future U.S. Program in Neutrino Oscillations”, submitted by the Neutrino Scientific Assessment Group. [http://www.science.doe.gov/hep/hepap\\_reports.shtml](http://www.science.doe.gov/hep/hepap_reports.shtml)
- [31] A. Rubbia, “Experiments for CP-violation: A giant liquid argon scintillation, Cerenkov and charge imaging experiment?,” arXiv:hep-ph/0402110.
- [32] Letter of Intent in preparation. See presentations by G. Rameika and N. Saoulidou at 2nd Project X workshop at Fermilab, [http://www.fnal.gov/directorate/Longrange/Steering\\_Public/Neutrinos.html](http://www.fnal.gov/directorate/Longrange/Steering_Public/Neutrinos.html)
- [33] B. Baibussinov *et al.*, “A new, very massive modular Liquid Argon Imaging Chamber to detect low energy off-axis neutrinos from the CNGS beam. (Project MODULAR),” arXiv:0704.1422 [hep-ph].
- [34] See FERMILAB-TM-2384-E (Oct 2006)
- [35] Portable Neon Purification System, R. Richardson and R. Schmitt, Advances in Cryogenic Engineering, 1995 and <http://lartpc-docdb.fnal.gov/cgi-bin/ShowDocument?docid=251>
- [36] Tests conducted at FNAL.
- [37] Measurements by Warp Collaboration to be published in NIM
- [38] P. Rehak, private communication
- [39] F. Arneodo *et al.* [ICARUS-Milano Collaboration], “Performance of a liquid argon time projection chamber exposed to the WANF neutrino beam,” arXiv:physics/0609205.
- [40] Fermilab FESS Project Definition Report, Engineering Project No. 6-7-82